

# UNC-108/RAB-2 and its effector RIC-19 are involved in dense core vesicle maturation in *Caenorhabditis elegans*

Marija Sumakovic,<sup>1</sup> Jan Hegemann,<sup>1</sup> Ling Luo,<sup>1</sup> Steven J. Husson,<sup>2</sup> Katrin Schwarze,<sup>1</sup> Christian Olendrowitz,<sup>1</sup> Liliane Schoofs,<sup>2</sup> Janet Richmond,<sup>3</sup> and Stefan Eimer<sup>1</sup>

<sup>1</sup>European Neuroscience Institute Goettingen, German Research Foundation Research Center for Molecular Physiology of the Brain, 37077 Goettingen, Germany

<sup>2</sup>Functional Genomics and Proteomics Unit, Biology Department, Catholic University of Leuven, BE-3000 Leuven, Belgium

<sup>3</sup>Department of Biological Sciences, University of Illinois at Chicago, Chicago, IL 60607

Small guanosine triphosphatases of the Rab family regulate intracellular vesicular trafficking. Rab2 is highly expressed in the nervous system, yet its function in neurons is unknown. In *Caenorhabditis elegans*, *unc-108/rab-2* mutants have been isolated based on their locomotory defects. We show that the locomotion defects of *rab-2* mutants are not caused by defects in synaptic vesicle release but by defects in dense core vesicle (DCV) signaling. DCVs in *rab-2* mutants are often enlarged and heterogeneous in size; however, their number

and distribution are not affected. This implicates Rab2 in the biogenesis of DCVs at the Golgi complex. We demonstrate that Rab2 is required to prevent DCV cargo from inappropriately entering late endosomal compartments during DCV maturation. Finally, we show that RIC-19, the *C. elegans* orthologue of the human diabetes autoantigen ICA69, is also involved in DCV maturation and is recruited to Golgi membranes by activated RAB-2. Thus, we propose that RAB-2 and its effector RIC-19 are required for neuronal DCV maturation.

## Introduction

Members of the Rab family of small GTPases organize virtually all aspects of intracellular membrane trafficking and are highly enriched in neurons (Zerial and McBride, 2001; Fukuda, 2008). They act as membrane-bound molecular switches cycling between an inactive GDP-bound form and an active GTP-bound form. Rab proteins function through a set of effector proteins to which they bind in their active form. Through their effectors, Rab GTPases regulate actin and microtubule-dependent transport, vesicle budding and tethering, and membrane fusion (Ng and Tang, 2008). Because Rab GTPases can bind to multiple effectors, they are able to regulate and integrate different trafficking events. Through sequential interactions of a Rab GTPase with different downstream effectors, directionality and proof-reading can be achieved during membrane transport. The activity

of Rab GTPases is temporally and spatially controlled through the action of guanine exchange factors and GTPase-activating proteins (Fukuda, 2008).

Rab GTPases are prime candidates to regulate synaptic activity as they have been shown to control both endo- and exocytosis events at the synapse (Star et al., 2005). Interestingly, a recent proteomic analysis of highly purified synaptic vesicles (SVs) revealed that a large set of other Rab GTPases can be co-purified with SVs (Takamori et al., 2006). This suggests that multiple Rabs might be needed for correct SV trafficking and regulated release.

To find new Rab members involved in neuronal membrane trafficking, we analyzed the expression pattern of all Rab GTPases in *Caenorhabditis elegans*. In agreement with previous studies, we found that UNC-108, the highly conserved RAB-2 homologue in *C. elegans*, shows a very strong neuronal expression (Lu et al., 2008; Mangahas et al., 2008), suggesting a

Correspondence to Stefan Eimer: seimer@gwdg.de

Abbreviations used in this paper: ACh, acetylcholine; DCV, dense core vesicle; DNC, dorsal nerve cord; GPCR, G protein-coupled receptor; HPF, high pressure freeze; HSN, hermaphrodite-specific neuron; iDCV, immature DCV; MALDI-TOF MS, matrix-assisted laser desorption ionization time of flight mass spectrometry; mDCV, mature DCV; NGM, Nematode growth medium; NMJ, neuromuscular junction; SV, synaptic vesicle; TFA, trifluoroacetic acid; VNC, ventral nerve cord.

© 2009 Sumakovic et al. This article is distributed under the terms of an Attribution-Noncommercial-Share Alike-No Mirror Sites license for the first six months after the publication date [see <http://www.jcb.org/misc/terms.shtml>]. After six months it is available under a Creative Commons License [Attribution-Noncommercial-Share Alike 3.0 Unported license, as described at <http://creativecommons.org/licenses/by-nc-sa/3.0/>].

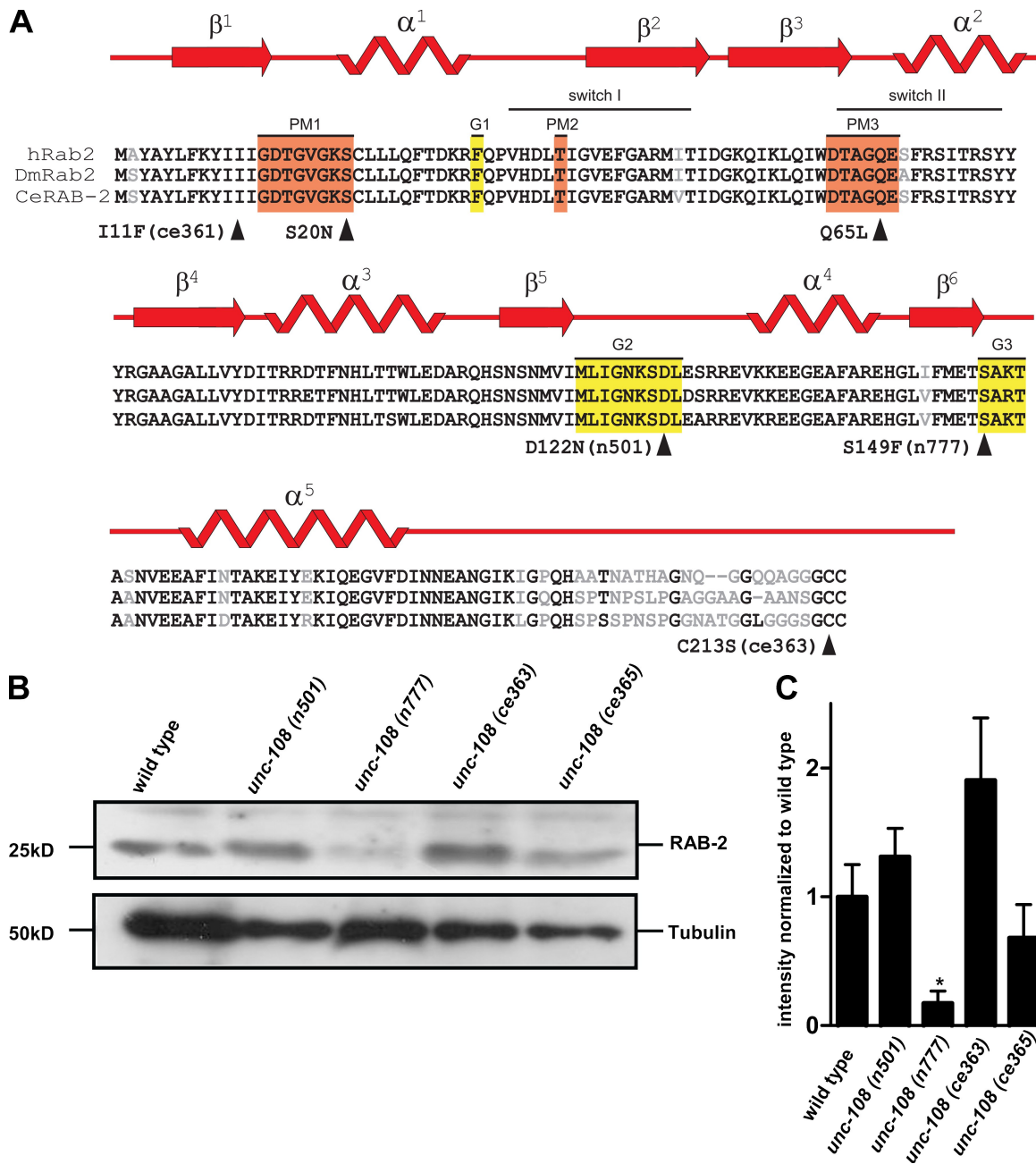


Figure 1. **UNC-108 is a homologue of human Rab2.** (A) Sequence alignment of Rab2 from *C. elegans*, *Homo sapiens*, and *Drosophila*. Domains responsible for phosphate and  $Mg^{2+}$  binding (orange boxes) and guanine moiety binding (yellow boxes) are shown. Arrowheads indicate point mutations within RAB-2. Mutations rendering RAB-2 constitutively inactive (S20N) and constitutively active (Q65L) are shown (Tisdale, 1999). (B) Western blot of protein extracts from different *unc-108* alleles probed with polyclonal RAB-2 antibodies. Tubulin loading control is also shown. (C) Quantification of normalized RAB-2 protein levels. Error bars = SEM (\*,  $P < 0.05$ ; Student's *t* test;  $n = 4$ ).

neuronal function. Although recent studies have focused on the role of UNC-108/RAB-2 in the removal of apoptotic cells (Lu et al., 2008; Mangahas et al., 2008) and glutamate receptor trafficking (Chun et al., 2008), the precise neuronal defect impairing locomotion was not investigated.

Rab2 has been shown to localize to the pre-Golgi vesicular tubular compartment and to be required for vesicular transport between the ER and the Golgi apparatus (Tisdale and Balch, 1996). Subsequently, active Rab2 was shown to also bind to Golgi matrix proteins and Golgi-localized coiled-coil proteins

(Short et al., 2001; Sinka et al., 2008). Thus, a more general function of Rab2 for Golgi trafficking was proposed. Therefore, it is surprising that *C. elegans unc-108/rab-2* mutants exhibit very specific locomotion defects more indicative of altered signaling at the neuromuscular junction (NMJ).

We report in this study that the locomotory defects of *unc-108/rab-2* mutants result, at least in part, from altered dense core vesicle (DCV) signaling in neurons as the result of defects during DCV biogenesis. RAB-2 activity is specifically required for the retention of cargo in DCVs during maturation, preventing

its removal to endosomal compartments. We further identify RIC-19, the *C. elegans* orthologue of the human diabetes autoantigen ICA69, as a key RAB-2 effector for DCV maturation in neuronal cell somas.

## Results

### UNC-108/RAB-2 mutations differentially affect protein function and stability

In *C. elegans*, UNC-108/RAB-2 is ubiquitously expressed but shows the strongest expression in neurons (Chun et al., 2008). The *unc-108* gene is defined by both dominant and recessive alleles, which all display similar locomotory defects. The two dominant *unc-108* alleles, *n501* (D122N) and *n777* (S149F), carry missense mutations within the conserved domains G2 and G3, respectively, which are required for binding of the guanine moiety of GTP or GDP (Fig. 1 A; Simmer et al., 2003). Recessive alleles of *unc-108* contain either missense mutations *ce363* (C213S) and *ce365* (I11F) (Lu et al., 2008; Mangahas et al., 2008) or a deletion *nu415* (Chun et al., 2008). The *nu415* deletion serves as null allele, as it removes the C terminus and is not detectable on Western blots. All other mutant RAB-2 proteins could be detected in mixed staged worm extracts by Western blotting using polyclonal mouse antibodies developed against *C. elegans* RAB-2 (Fig. 1 B). However, the protein levels of RAB-2 (*ce365*)I11F were slightly reduced, and the amount of RAB-2 (*n777*)S149F protein was strongly reduced by ~80% compared with wild type (Fig. 1, B and C). Because all mutant RAB-2 proteins were detectable in vivo, it is unlikely that differences in protein levels could account for the functional defects observed.

To analyze how the mutations affect RAB-2 protein function, we used recombinant GST fusion proteins to determine their biochemical properties, including GTP hydrolysis rates and GTP affinity. As a control, we used the RAB-2 mutants S20N (impaired in nucleotide exchange and reduced affinity for GTP) and Q65L (dominantly active because of a lack of GTPase activity but not GTP binding; Tisdale, 1999; Spinosa et al., 2008).

Both dominant RAB-2 mutations S149F (*n777*) and D122N (*n501*) affected two loops that coordinate the guanine nucleotide; therefore, it is likely that GTP binding was affected (Fig. 2 A). Although both mutations led to an increase in the affinity for GTP (Fig. 2 C), only the *n501* mutation prevented the hydrolysis of GTP (Fig. 2 B). Thus, the D122N (*n501*) mutant RAB-2 behaves similar to the constitutively active Q65L mutant (Fig. 2, B and C). Therefore, RAB-2 *n777* and *n501* can be considered constitutively active. Thus, biochemically, *n777* and *n501* can be clearly distinguished from the recessive loss-of-function mutation I11F (*ce365*), which displayed wild type-like GTP affinity and hydrolysis rates (Fig. 2, B and C).

### UNC-108/RAB-2 mutations do not affect SV release

*unc-108*(*n777*) and (*n501*) mutations cause dominant locomotory defects (Park and Horvitz, 1986; Simmer et al., 2003; Chun et al., 2008), reducing locomotion in heterozygous and homozygous strains by ~50% as compared with the wild type (Fig. 3 A). Impaired locomotion suggests defects in synaptic transmission at

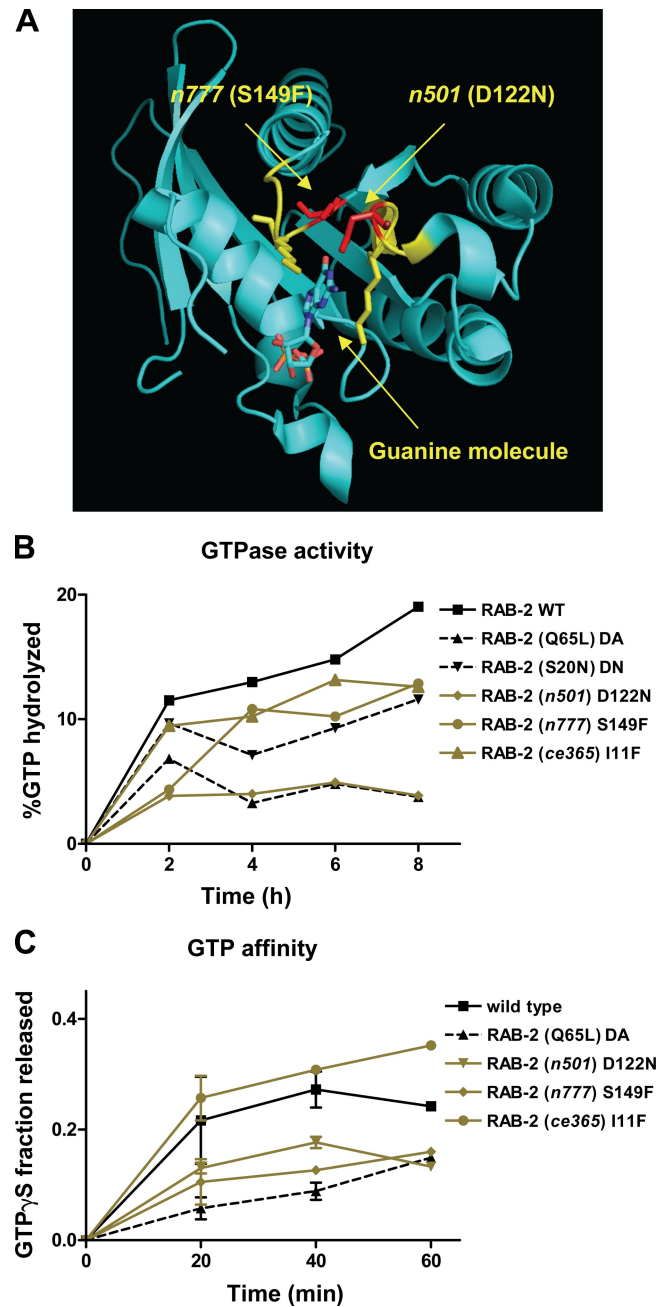


Figure 2. RAB-2 mutations change the biochemical properties of the protein. (A) Rab2 structure with guanine-binding domain labeled in yellow. The altered amino acids in dominant *unc-108* mutants are red. (B) GTP hydrolysis rates were determined in vitro using recombinant RAB-2 ( $n = 3$  per time point). (C) GTP affinity of recombinant RAB-2 using nonhydrolyzable  $\gamma$ -[ $^{35}$ S]GTP. Error bars = SEM ( $n = 9$  per time point).

NMJs. Therefore, we tested the cholinergic signaling at NMJs by assaying the response of the dominant *unc-108* mutants to the acetylcholine (ACh) esterase inhibitor aldicarb. Aldicarb prevents the removal of ACh from the synaptic cleft by inhibiting ACh esterase, leading to chronic stimulation of the postsynaptic receptors, resulting in paralysis of the animal (Miller et al., 1996). *n777* and *n501* mutants display a reduced sensitivity to aldicarb as compared with wild type (Fig. 3 B). The aldicarb resistance of *n777* and *n501* is comparable with that of *rab-3* mutants, which

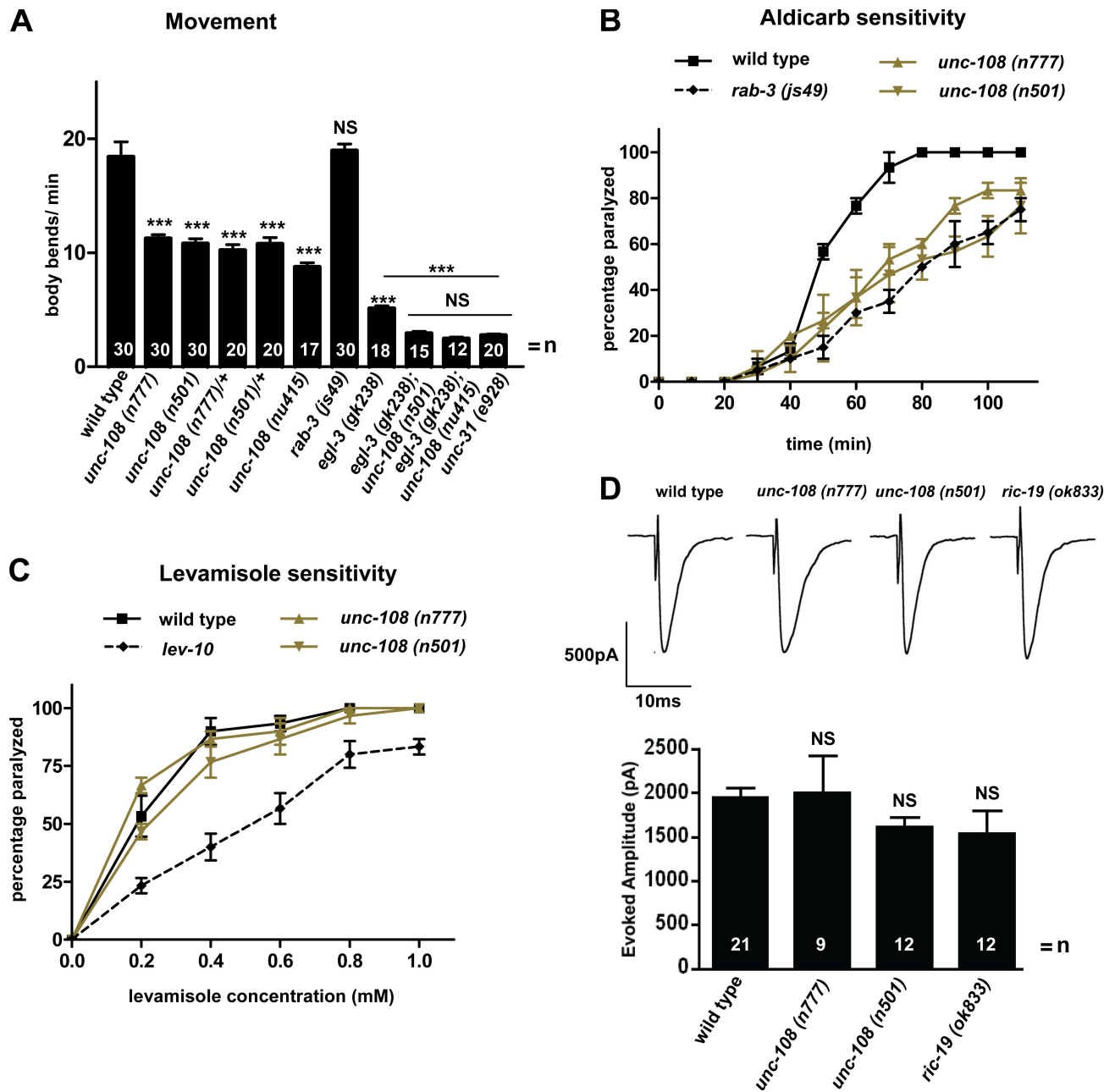


Figure 3. *unc-108* mutants have reduced locomotion and aldicarb sensitivity but not SV release at the NMJ. (A) The locomotory defects of *unc-108* mutants are synthetically enhanced in *unc-108; egl-3* double mutants to the level of *unc-31/CAPS*. Error bars = SEM (\*\*\*,  $P < 0.005$ ; Student's  $t$  test; all strains were compared with wild type; double mutants are compared with *egl-3* and *unc-31* single mutants). (B and C) Dominant *unc-108* mutants are resistant to the ACh esterase inhibitor aldicarb (B), similar to *rab-3*, and exhibit a wild type-like sensitivity to the postsynaptic nicotinic receptor agonist levamisole (C). The weakly levamisole-resistant *lev-10* mutant is shown as control. Error bars = SEM ( $n = 30$ ). (D) The evoked release of SVs at the NMJ is similar between wild type and dominant *unc-108* and *ric-19* mutants. Error bars = SEM.

have been shown to have defects in SV tethering (Gracheva et al., 2008). To test whether the reduced sensitivity to aldicarb is caused by a functional impairment of the postsynaptic site, we directly activated postsynaptic ACh receptors by applying levamisole. The anthelmintic drug levamisole is an agonist for levamisole-sensitive ACh receptors, leading to paralysis (Richmond and Jorgensen, 1999; Gally et al., 2004). *unc-108* mutants displayed a wild type-like sensitivity to increasing concentrations of levamisole (Fig. 3 C) and were clearly distinguishable from the levamisole resistance of *lev-10* mutants, which lack clustered levamisole

receptors (Gally et al., 2004). We conclude that postsynaptic levamisole-sensitive receptors are largely unaffected by the dominant *unc-108* mutations. To directly test whether dominant *unc-108* mutants exhibit altered synaptic transmission, evoked responses were obtained from the NMJ of dissected worms. The mean amplitude of evoked release was not significantly different from wild type in either *n777* or *n501* (Fig. 3 D). From these data, we conclude that changes in cholinergic signaling are unlikely to account for the sluggish locomotion and aldicarb resistance of the dominant *unc-108* mutants.

### No ultrastructural defects at the NMJ in *unc-108* mutants

The reduced locomotion *unc-108* mutants could be a consequence of developmental defects or changes in the number or shape of synapses. However, no change in GABAergic motor neuron number or morphology was detected (Fig. S2 A). Furthermore, by analyzing the accumulation of synaptobrevin-GFP (SNB-1-GFP)-labeled SVs, we showed that the synapse number, shape, and spacing of cholinergic motor neurons projecting axons into the dorsal cord were also comparable with wild type (Fig. S2 B). Therefore, it is unlikely that the behavioral defects in the dominant *unc-108* mutants are caused by defects in motor neuron development or synapse formation.

To exclude ultrastructural changes at the synapse of *unc-108* mutants, we studied the morphology of presynaptic terminals by high pressure freeze (HPF) EM (Rostaing et al., 2004). As shown in Fig. 4 A, the ultrastructure of the active zone as well as the size of SVs were similar to wild type for both the dominant and the recessive *unc-108* alleles (Fig. 4 A and Table I). Differences in the distribution of SVs relative to the presynaptic density can also lead to reduced SV exocytosis and thus aldicarb resistance, as seen in *rab-3* mutants (Gracheva et al., 2008). An HPF EM analysis of the SV distribution in motor neurons of *unc-108* mutants revealed that the number and distribution of SVs were similar to wild type and clearly distinguishable from *rab-3* (Fig. 4, A and B; and Table I). In addition, a precise analysis of the SV distribution directly at the presynaptic density, distinguishing between SVs at the density versus SVs at the membrane, also revealed no differences between *unc-108* mutants and wild type (unpublished data). Furthermore, the mean synaptic area of cholinergic motor neurons as well as the size of SVs were also not affected (Table I). Therefore, we conclude that the ultrastructure as well as the SV distribution are unaffected in *unc-108* mutants carrying either recessive (*ce363*, *ce365*, and *nu415*) or dominant alleles (*n777* and *n501*; Table I). These data are consistent with wild type-evoked responses observed in all *unc-108* mutants (Fig. 3 D; see Edwards et al. in this issue), suggesting that SV secretion is not, per se, affected by *unc-108/rab-2* mutations.

### *unc-108* mutants are defective in DCV signaling

The lack of any detectable defects in synaptic transmission prompted us to investigate DCV signaling at the NMJ. In addition to SVs, DCVs are secreted from motor neurons. Defects in DCV release, like in the *unc-31/CAPS* mutant, can also lead to slow locomotion similar to *unc-108* mutants (Gracheva et al., 2007). To analyze DCVs in *unc-108* mutants, we used a strain stably expressing a fusion protein between the neuropeptide NLP-21 precursor fused to YFP (NLP-21-YFP) in cholinergic motor neurons. It has been previously demonstrated that NLP-21-YFP-derived fusion proteins are packaged into DCVs, transported to axons, and released into the body cavity (Sieburth et al., 2007). Once secreted, NLP-21-derived YFP is subsequently endocytosed by six scavenger cells, the coelomocytes, in the body cavity. Thus, the level of YFP fluorescence taken up by coelomocytes can be a direct measure for the amount of YFP fusion protein released.

In both dominant *unc-108* mutants, the YFP intensity in axons was strongly reduced by  $65 \pm 4\%$  (*n777*) and  $80 \pm 2\%$  (*n501*) as compared with wild type (Fig. 5 A). We obtained similar results using the *unc-108(nu415)* null mutant (Fig. 5 A). The reduction of NLP-21-YFP fluorescence in axons can be rescued by expression of RAB-2 specifically in cholinergic DA motor neurons (unpublished data). Furthermore, the decreased cargo levels in axons are not restricted to NLP-21-YFP because tagging FLP-3 or atrial natriuretic factor neuropeptides results in similarly reduced YFP levels in *unc-108* mutant axons (Edwards et al., 2009). To test whether the tagged neuropeptide cargo is properly secreted in *unc-108* mutants, we measured the intensity of the YFP fluorescence internalized by the coelomocytes and found that it was also decreased by  $62 \pm 7\%$  for *n777* and  $76 \pm 2\%$  for *n501* (Fig. 5 B). Because neither *unc-108* gain-of-function mutation affected the uptake of soluble secreted GFP by coelomocytes (Fig. S5), the coelomocyte fluorescence intensity could be used as an accurate readout for DCV exocytosis. Because in *unc-108* mutants the NLP-21-derived YFP taken up by the coelomocytes is reduced to the same levels as the YFP content in axonal DCVs, we conclude that DCV exocytosis by itself is largely unaffected in *unc-108/rab-2* mutants.

The reduction of synaptic NLP-21-YFP fluorescence in *unc-108* mutants could be caused by a reduction either in the number or content of DCVs. To distinguish between these possibilities, we analyzed synaptic DCV number in motor neurons by HPF EM (Fig. 4 A). For the dominant alleles, the number of DCVs at the synapse was similar to wild type (Table I), and their distribution was unaffected (not depicted). This suggests that the decrease of axonal NLP-21-YFP fluorescence is specifically caused by DCVs containing less NLP-21-derived YFP, which would be consistent with less YFP being secreted from motor neurons.

The loss-of-function alleles exhibited mild but variable reductions of DCVs number per synaptic profile, as analyzed by EM, ranging from 40% in *ce363* to 15% in *nu415* (Table I). However, importantly, the measured reduction of DCVs in the *nu415* null allele was not statistically significant when compared with wild type. However, the mean diameter of the DCVs in some of the loss- and gain-of-function alleles was slightly, but significantly, increased (Table I). This strongly points to an involvement of RAB-2 in DCV maturation.

### RAB-2 localizes to the Golgi apparatus but not to synapses

To understand how RAB-2 affects DCV biogenesis or maturation, we studied its subcellular localization. N-terminally fused monomeric YFP (mYFP)- or mCherry-RAB-2 localized to discrete cytoplasmic puncta in cell bodies of motor neurons (Fig. 6 A). The localization of RAB-2 fusion proteins overlapped with general Golgi markers such as  $\alpha$ -mannosidase II or COPI vesicles (Fig. 6 A). However, RAB-2 did not colocalize with markers of the ER (cytochrome b5) or early endosomes (FYVE domain of EEA-1). We also wanted to confirm the localization by analyzing the endogenous RAB-2 protein. For this purpose, we generated monoclonal antibodies against *C. elegans* RAB-2 and localized the endogenous RAB-2 in motor neurons on HPF

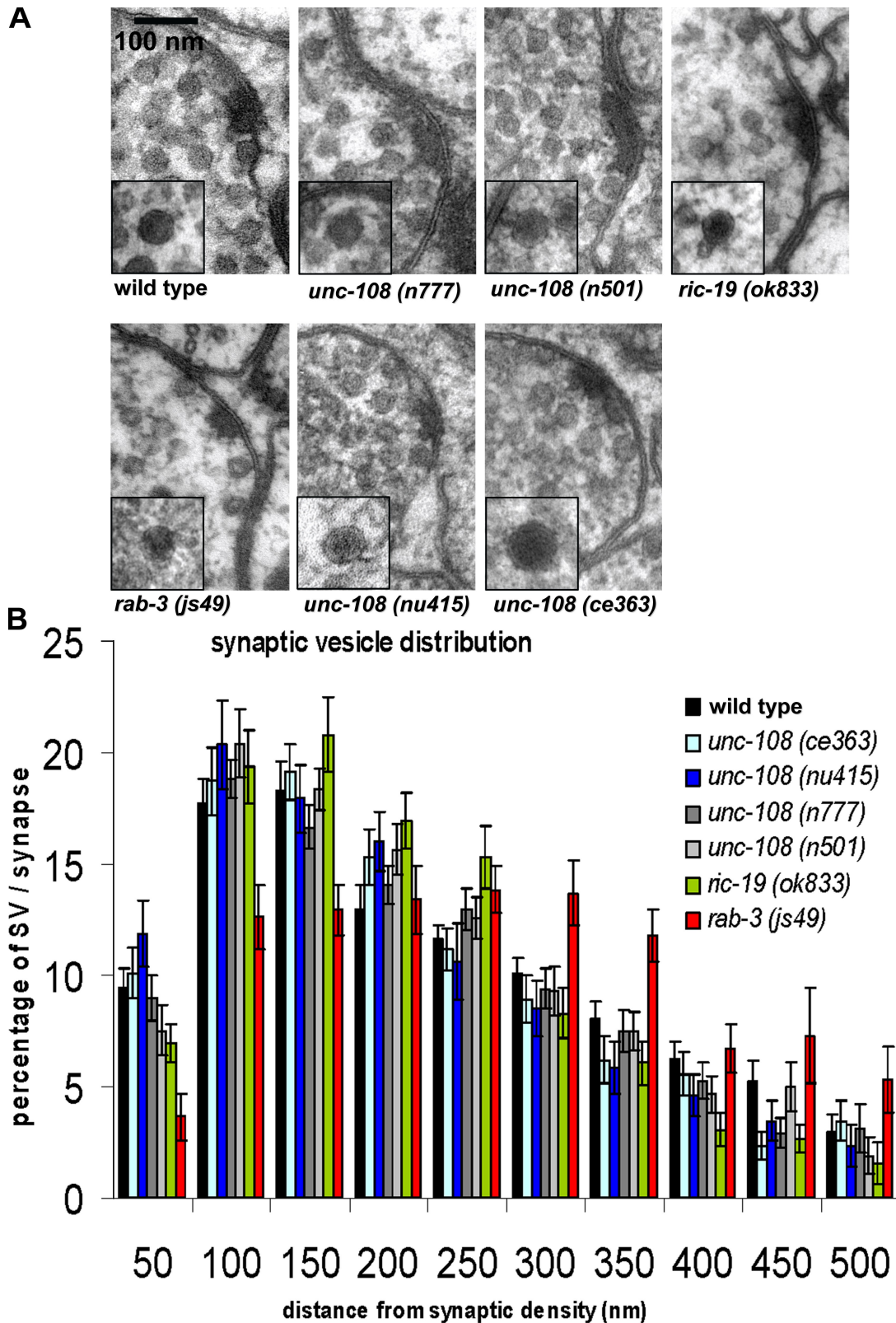


Figure 4. *unc-108* mutants have normal synaptic morphology and SV distribution. (A) The morphology of motor neuron synapses in the DNC in different *C. elegans* strains is shown in 40-nm HPF EM cross sections, with electron micrographs of a single DCV section shown in the insets. (B) SV distribution relative to the presynaptic density was analyzed for *unc-108* and *ric-19* mutants, and a tethering-defective *rab-3* mutant is shown as a control. *unc-108* and *ric-19* SV distributions are not significantly different compared with wild type (one way analysis of variance with Dunnett's posttest). Error bars = SEM.

Table 1. SV and DCV statistics

Genotype	Number of profiles/animals analyzed	Mean synaptic area	SV/profile	Mean diameter of SVs	DCV/profile	Mean diameter of DCVs
		$\mu\text{m}^2$		nm		nm
Wild type	30/5	0.25 $\pm$ 0.02	34.9 $\pm$ 2.4	30.3 $\pm$ 0.7	2.0 $\pm$ 0.2	44.8 $\pm$ 1.0
<i>unc-108(n777)</i>	34/4	0.20 $\pm$ 0.01	39.3 $\pm$ 1.8	28.4 $\pm$ 0.7	2.0 $\pm$ 0.2 <sup>a</sup>	54.1 $\pm$ 3.4 <sup>c</sup>
<i>unc-108(n501)</i>	31/4	0.23 $\pm$ 0.03	38.7 $\pm$ 1.7	27.7 $\pm$ 0.5	2.3 $\pm$ 0.3 <sup>a</sup>	49.4 $\pm$ 2.3 <sup>b</sup>
<i>unc-108(ce363)</i>	28/3	0.25 $\pm$ 0.02	35.1 $\pm$ 2.8	30.3 $\pm$ 0.7	1.2 $\pm$ 0.3 <sup>b</sup>	71.8 $\pm$ 3.4 <sup>d</sup>
<i>unc-108(nu415)</i>	26/4	0.21 $\pm$ 0.01	29.2 $\pm$ 1.5	26.6 $\pm$ 0.6	1.7 $\pm$ 0.4 <sup>a</sup>	46.9 $\pm$ 2.0 <sup>a</sup>
<i>ric-19(ok833)</i>	32/4	0.22 $\pm$ 0.01	33.1 $\pm$ 1.3	27.2 $\pm$ 0.6	2.7 $\pm$ 0.4 <sup>a</sup>	42.0 $\pm$ 2.0 <sup>a</sup>
<i>rab-3(js49)</i>	13/3	0.22 $\pm$ 0.02	37.7 $\pm$ 3.4	27.8 $\pm$ 0.6	3.2 $\pm$ 0.5 <sup>b</sup>	41.7 $\pm$ 1.1 <sup>b</sup>

SV and DCV numbers and diameters are as determined by HPF EM. DCV statistics of *unc-108* mutants are compared with wild type (Student's *t* test).

<sup>a</sup>NS.

<sup>b</sup>P < 0.05.

<sup>c</sup>P < 0.01.

<sup>d</sup>P < 0.005.

immuno-EM thin plastic sections. As seen in Fig. 6 B, RAB-2 is broadly localized to the Golgi complex with some preference for the early Golgi cisternae. While analyzing 14 neuronal Golgi complexes, we found, on average, 3.3  $\pm$  0.9 immunogold labels on the cis side, 1.8  $\pm$  0.5 within the medial Golgi, and 1.1  $\pm$  0.4 on the trans side. However, some RAB-2 immunogold labeling was also seen on vesicular structures surrounding the Golgi (Fig. 6 B and Fig. S3 E). This RAB-2 staining was specific because it was absent in the *nu415* deletion mutant (Fig. S3 F). Immunogold staining was also detectable on vesicular structures in axons; however, no specific RAB-2 staining was detected on SVs or DCVs or directly at the active zone (unpublished data). Similarly, mCherry–RAB-2 was not detected at synapses of motor neurons projecting axons into the dorsal nerve cord (DNC) or at the synapses between the hermaphrodite-specific neuron (HSN) and vulva muscles (Fig. 6 C). Therefore, the localization data suggest that RAB-2 functions in neuronal cell somas, including membrane compartments at and around the Golgi and in axons. However, RAB-2 is not required to maintain the structural integrity of the Golgi because the morphology of Golgi complexes in dominant or recessive *unc-108* mutants appeared normal when compared with wild type using HPF EM (Fig. S3, A–D).

#### Neuropeptides are processed normally in *unc-108* mutants

The Golgi localization of RAB-2 in the cell soma and our finding that *unc-108* mutant DCVs have a strong deficiency in a soluble cargo protein led us to investigate events related to DCV maturation in *unc-108* mutants. Neuropeptides are packaged into DCVs at the Golgi as precursors along with their processing enzymes, furin type of proprotein convertases, carboxypeptidases, and amidation enzymes (Husson et al., 2007b). After cleavage from their precursor, neuropeptides are concentrated and aggregated within maturing DCVs. Moreover, the vesicles must be properly acidified to activate the processing enzymes (Kim et al., 2006; Morvan and Tooze, 2008). To investigate neuropeptide processing, we analyzed neuropeptide content in three independent protein extracts, from wild type and *unc-108(n777)*

and (*n501*) mutants, by high performance liquid chromatography and matrix-assisted laser desorption ionization time of flight mass spectrometry (MALDI-TOF MS). It has been shown that neuropeptide processing defects can clearly be distinguished by this method (Husson et al., 2006, 2007a). As shown in Table S1, all detectable neuropeptides are correctly and fully processed in the dominant *unc-108* mutants, including neuropeptide-like protein (NLP)-type neuropeptides, as well as the C-terminally modified FMRamide-like peptides (FLPs; Li et al., 1999). Thus, the processing of neuropeptides is not defective in *unc-108* mutants. The MALDI-TOF MS method used to analyze and detect neuropeptide in protein extracts from *C. elegans* is not quantitative and therefore allows only qualitative conclusions.

To test whether mutations in RAB-2 affect neuropeptide levels, we analyzed double mutants of *unc-108/rab-2* with *egl-3*, a proprotein convertase required for proteolytically liberating neuropeptides from their precursor (Kass et al., 2001). In the absence of EGL-3 activity, no active neuropeptides were detectable (Husson et al., 2006). If *egl-3* and *unc-108* are involved in the same pathway required for neuropeptides, an *egl-3; unc-108* double mutant should display the same phenotype as *egl-3* single mutants. However, *egl-3; unc-108* double mutants showed a strong enhancement of the locomotory defects, reducing locomotion to the level of an *unc-31/CAPS* mutant, which is defective in DCV release (Fig. 3 A). Both dominant and recessive *unc-108* alleles showed the same strong synthetic interaction with *egl-3*. This suggests that *unc-108* and *egl-3* act in parallel pathways for DCV signaling. Thus, it is unlikely that *unc-108* mutations strongly affect neuropeptide signaling, which is in agreement with our MALDI-TOF MS analysis.

#### RAB-2 mutations affect DCV maturation

DCVs are generated at the late Golgi, most likely within the TGN (Kim et al., 2006; Morvan and Tooze, 2008). Neuropeptide precursors, processing enzymes, and accessory proteins needed for DCV exocytosis have to be sorted into transport vesicles that subsequently bud off the Golgi apparatus. However, during the sorting and packaging process, constitutive secretory cargo, lysosomal enzymes, and other membrane proteins are

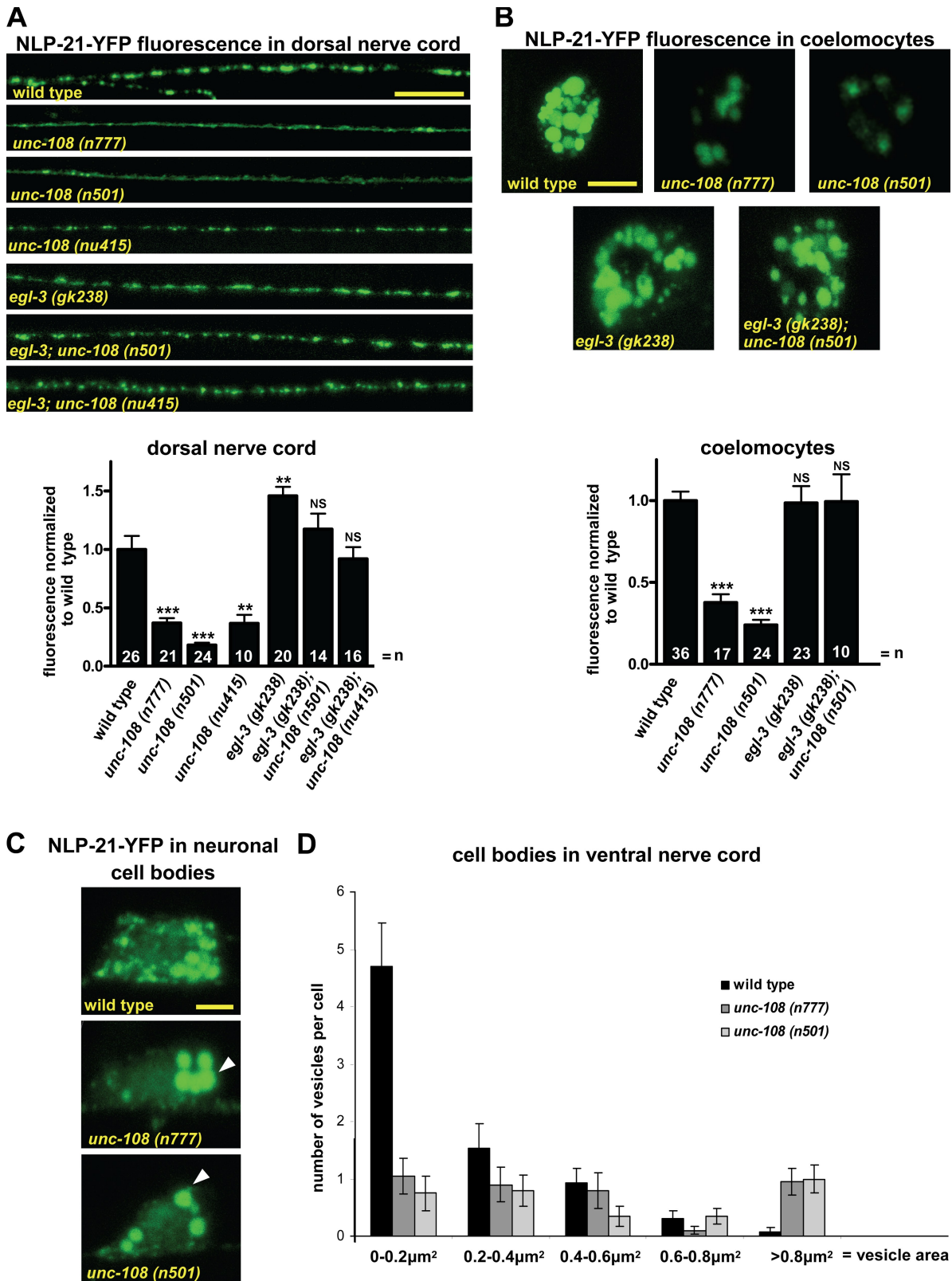
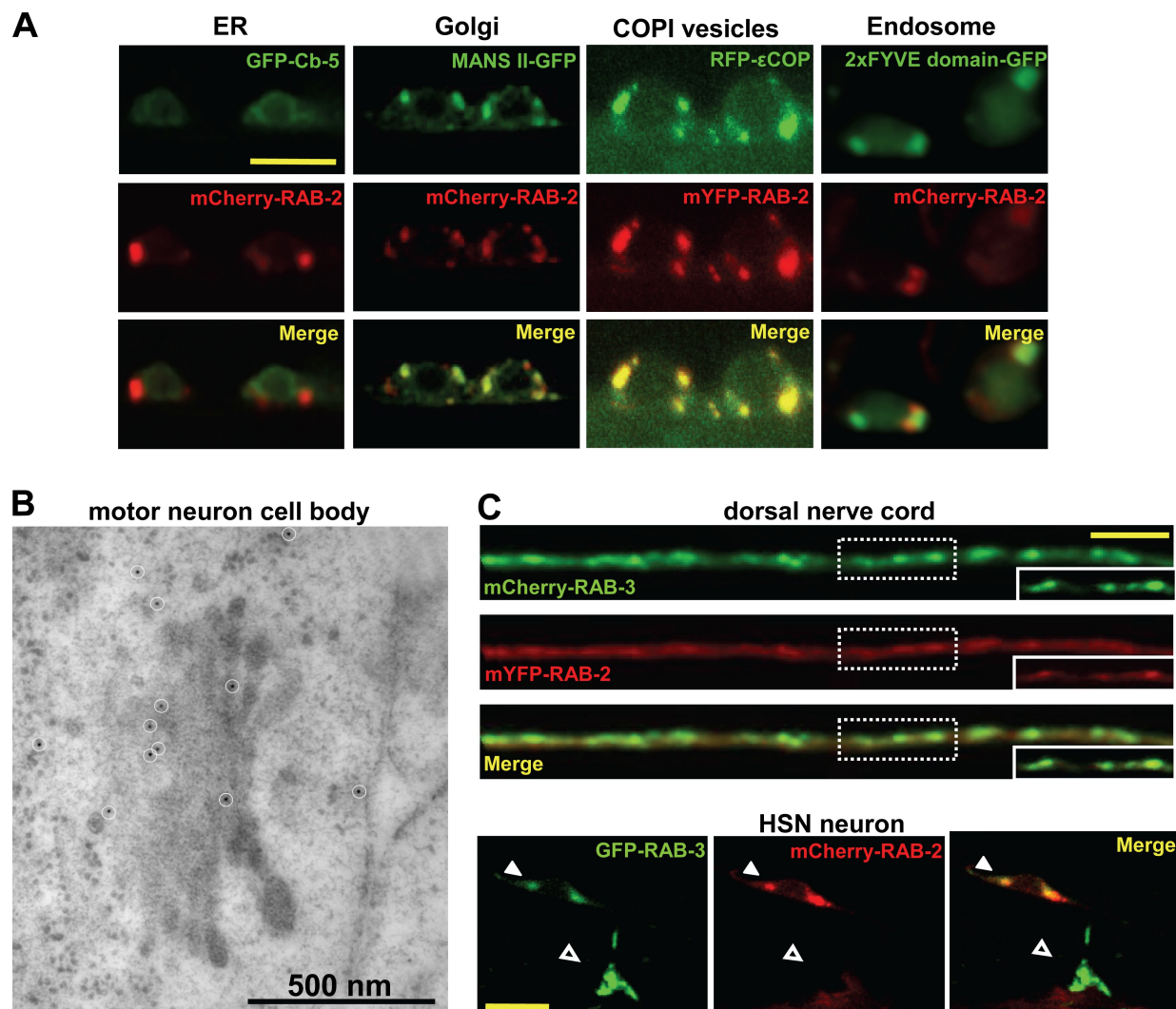


Figure 5. *unc-108* mutant DCVs contain less soluble cargo. (A) Animals carrying integrated array *nuls183* are expressing NLP-21-YFP in motor neurons projecting axons into the DNC. Representative images of the synaptic accumulation of DCVs with YFP-tagged NLP-21 neuropeptide in the DNC in the respective genetic backgrounds are shown. Mean fluorescence was normalized to wild type (graph below). The absence of EGL-3 leads to strong accumulation of neuropeptides at the synapse and restores wild-type levels in both dominant and recessive *unc-108* alleles. Error bars = SEM (\*\*,  $P < 0.01$ ; \*\*\*,  $P < 0.005$ ; Student's *t* test). (B) Once released from axons, NLP-21-derived YFP is taken up by coelomocytes. Mean coelomocyte fluorescence in various mutants was normalized to wild type (graph below). Error bars = SEM (\*\*\*,  $P < 0.005$ ). (C and D) NLP-21-YFP fluorescence in motor neuron somas in the VNC are shown, and size distribution of NLP-21-YFP-positive vesicles in neuronal cell bodies of dominant *unc-108* mutants is compared with wild type. Arrowheads point to vesicles with surface area  $>0.8 \mu\text{m}^2$ . Error bars = SEM ( $n = 10$ ). Bars: (A)  $10 \mu\text{m}$ ; (B)  $5 \mu\text{m}$ ; (C)  $2 \mu\text{m}$ .



**Figure 6. RAB-2 localizes to the Golgi apparatus and is not present at the synapses.** (A) Confocal images of motor neuron cell bodies expressing fluorescently tagged RAB-2 along with different intracellular markers are shown. RAB-2 extensively colocalizes with the Golgi marker mannosidase II (MANS II) and COPI-positive structures. RAB-2 shows no or only partial colocalization with the ER (cytochrome b5) or early endosomes (FYVE domain of EEA-1). (B) Immunogold labeling (white circles) of endogenous RAB-2 in motor neuron cell bodies showed staining at the Golgi complex and vesicular structures around the Golgi. (C) mYFP-RAB-2 (red) does not accumulate at the synapses in the DNC-like mCherry-RAB-3 (green). The dashed boxes represent the magnified synaptic puncta demonstrating no accumulation of RAB-2 at the synapses. In HSN neurons, mCherry-RAB-2 is present only in cytoplasmic puncta in the neuronal cell body (closed arrowheads) but not at the synapse with vulval muscles (open arrowheads). HSN synapses are labeled by GFP-RAB-3. Bars: (A) 5  $\mu\text{m}$ ; (C) 10  $\mu\text{m}$ .

copackaged into DCV precursors, forming immature DCV (iDCVs). To become fully functional, this inappropriate cargo has to be removed by clathrin-mediated membrane trafficking and delivered to the endosomal system. This remodeling allows for iDCV maturation into a mature DCV (mDCV).

In *unc-108* mutants, this process is likely to be perturbed. Indeed, although the number of DCVs did not change in dominant *unc-108* mutants, the DCVs contained less NLP-21-YFP-derived cargo. One possibility is that after the processing of the NLP-21-YFP fusion protein, the soluble YFP is less efficiently retained in iDCV and is sorted to the endosomal system during maturation. Therefore, one would expect to see aberrant NLP-21-YFP accumulation in the cell bodies of *unc-108* mutants. As shown in Fig. 5 (C and D), the neuronal cell bodies of *unc-108* mutants contained mostly large NLP-21-YFP-positive vesicular structures, as opposed to the small vesicles seen in wild type.

These structures often reached sizes  $>0.8 \mu\text{m}^2$ , which were never observed in wild-type neuronal cell bodies. To determine the identity of these NLP-21-YFP-positive vesicular structures, we tested their colocalization with various subcellular markers. In wild-type neuronal cell bodies of the ventral nerve cord (VNC), most of the NLP-21-YFP overlapped with RAB-2 and the early endosomal marker RAB-5 (Fig. 7 A). Almost no overlap was seen with the late endosomal marker RAB-7 or the lysosomal marker LMP-1. This suggests that most of the NLP-21-derived YFP accumulated at the Golgi and early endosomes.

This picture changed dramatically in the dominant *unc-108* mutants, where NLP-21-YFP largely overlapped with markers for late endosomes and lysosomes (Fig. 7 B). This supports the idea that in dominant *unc-108* mutants, the NLP-21-derived YFP is partially lost from maturing DCVs through the late endosomal-lysosomal degradation route. The step at which the

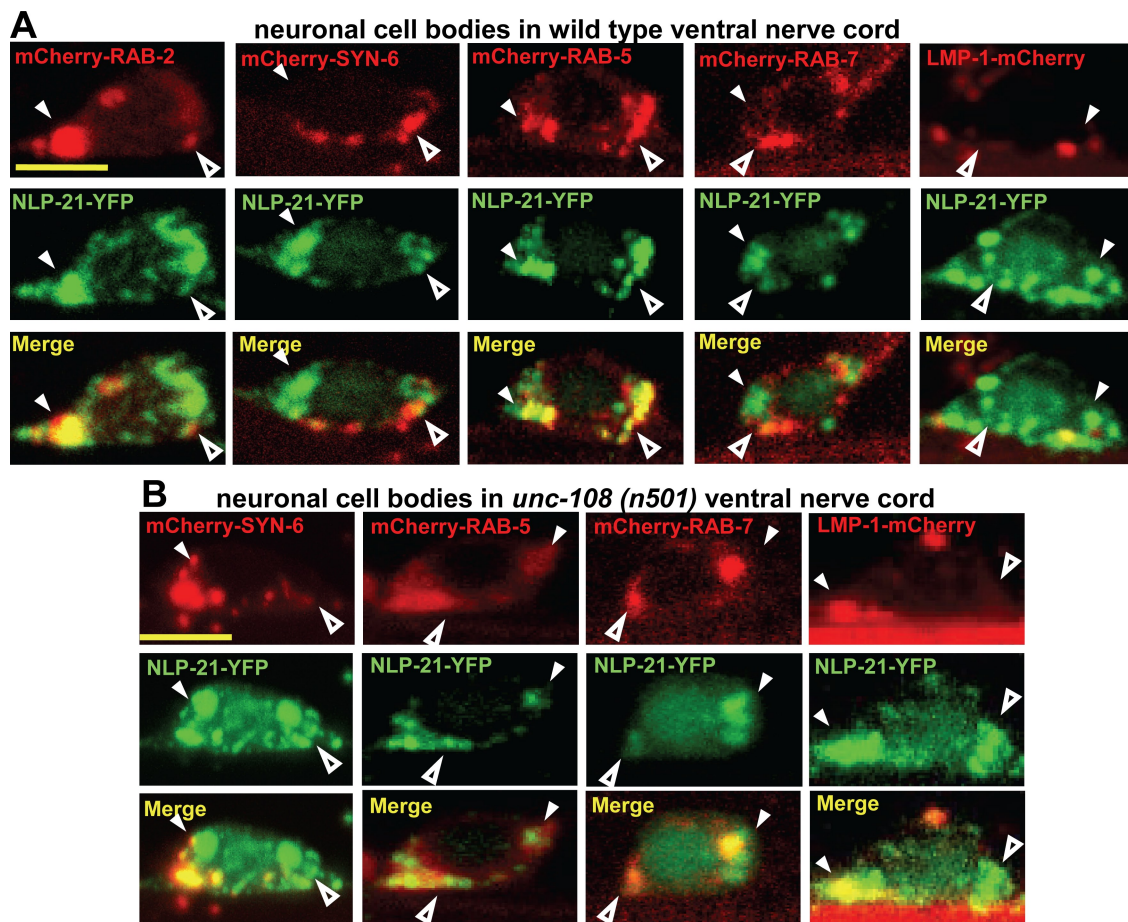


Figure 7. In *unc-108*, NLP-21-YFP enters the late endosomal compartment. (A and B) To identify NLP-21-YFP-positive vesicular structures in wild type (A) and *unc-108(n501)* strains (B) carrying the NLP-21-YFP integrated array, different intracellular markers were expressed panneuronally: RAB-2, syn-6 (iDCVs), RAB-5 (early endosome), RAB-7 (late endosome), and LMP-1 (lysosome). The closed and open arrowheads represent larger and smaller vesicular structures, respectively. NLP-21-YFP-positive vesicles in the *unc-108(n501)* strain mostly colocalize with the early endosomal marker RAB-5. Bars, 2  $\mu$ m.

soluble YFP cargo is lost in *unc-108* mutants occurs after peptide processing because blocking peptide processing with a null mutation in the EGL-3/PC2 convertase restores wild-type levels of the YFP cargo in *unc-108* axons (Fig. 5, A and B).

To test the hypothesis that the soluble YFP cargo is lost from the maturing DCV via the endosomal system, we interfered with early endosomal function by expressing the GTP-bound form RAB-5(Q78L)DA in neurons. As seen in Fig. 8 (A and B), the YFP fluorescence levels at the synapse were specifically rescued in *unc-108(n501)* mutants. In contrast, expression of RAB-5(Q78L)DA in wild-type motor neurons had no effect on axonal levels of the NLP-21-derived YFP fluorescence. In agreement with this, the NLP-21-derived YFP fluorescence was also rescued to wild-type levels in neuronal cell bodies of *unc-108(n501)* by expression of RAB-5(Q78L)DA (Fig. 8, C and D). These results confirm that during DCV maturation, RAB-2 activity is required for retaining specific cargo in maturing DCVs by preventing its entry to the late endosomal system.

#### RAB-2 cooperates with its effector RIC-19 during DCV maturation

Recently, it has been shown that in insulinoma cells, the diabetes autoantigen ICA69 acts as a RAB-2 effector involved in

insulin secretion (Spitzenberger et al., 2003; Buffa et al., 2008). Its *C. elegans* orthologue, RIC-19, is exclusively expressed in neurons (Pilon et al., 2000). Therefore, we reasoned that RIC-19, like RAB-2, might also function during DCV maturation. Similar to *unc-108* mutants, *ric-19(ok833)* deletion mutants displayed reduced locomotion and aldicarb resistance (Fig. 9, A and B), which could be rescued by neuronal *ric-19* expression. This suggests that RIC-19 might be required for efficient signaling at the NMJ.

Like for *unc-108*, both the morphology and the number and distribution of SVs were similar to wild type, as judged by EM (Fig. 4 and Table I). Consistent with this, the evoked release in *ric-19* mutants was not significantly reduced (Fig. 3 D), suggesting that SV function was normal. In contrast, *ric-19(ok833)* mutants showed a  $43 \pm 4\%$  reduction in the NLP-21-YFP fluorescence in DNC axons (Fig. 9, C and D) as well as a corresponding  $46 \pm 2\%$  reduction of NLP-21-derived YFP secretion, as judged by coelomocyte fluorescence (Fig. 9, F and G). Both defects were completely rescued by neuronal expression of *ric-19* (Fig. 9, C, D, and G). Furthermore, the appearance of large NLP-21-YFP-filled vesicular structures could also be seen in cell bodies of *ric-19* mutant motor neurons, accompanied by the disappearance of smaller vesicular structures (Fig. S4).

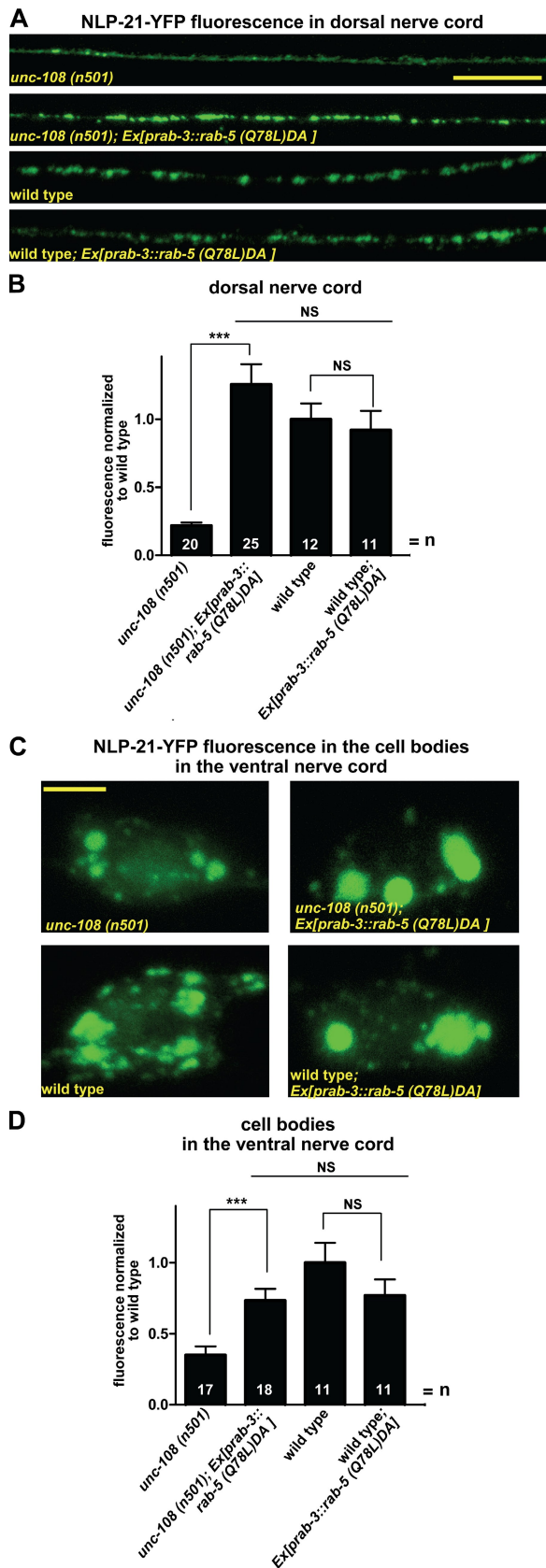


Figure 8. Overexpression of constitutively GTP-bound RAB-5 rescues the DCV maturation defects of *unc-108* mutants. (A and B) GTP-restricted RAB-5(Q78L)DA was expressed panneuronally in the NLP-21-YFP-expressing strain *nuls183* in wild type and *unc-108* mutants. RAB-5(Q78L)DA

Thus, *ric-19* mutants phenocopy dominant *unc-108/rab-2* mutants, which strongly suggests that RIC-19 and RAB-2 function in the same pathway required for DCV maturation.

*ric-19* and *unc-108* are both located on chromosome I and are only separated by 45 kb. Therefore, we used RNAi to show that *unc-108* and *ric-19* are in the same pathway required for DCV maturation. RNAi-mediated knockdown of RIC-19 by bacterial feeding in *unc-108* mutants did not enhance the movement defects (Fig. 9 A) nor the loss of NLP-21-YFP fluorescence in the DNC axons (Fig. 9, C and D). The RIC-19 RNAi was clearly functional because we could reproduce the loss of NLP-21-YFP fluorescence in wild-type animals by RIC-19 RNAi (Fig. 9, C and D) and also the down-regulation of endogenous RIC-19, as shown by Western blotting (Fig. 9 E). This highly suggests that RAB-2 affects DCV maturation via RIC-19.

To determine whether RIC-19 is a direct effector of RAB-2, we coexpressed RIC-19 with either wild-type or GTP-restricted (DA) or GDP-bound constitutively inactive (DN) HA-tagged RAB-2 forms in HeLa cells and immunoprecipitated RAB-2 using anti-HA antibodies. RIC-19 could be specifically affinity purified with RAB-2(Q65L)DA and to a lesser extent with wild-type RAB-2 (Fig. 10 A) but not with the inactive form RAB-2(S20N)DN, suggesting that RIC-19 is indeed an effector of RAB-2.

The endogenous RIC-19 protein levels were unaffected in *unc-108* mutants, as judged by Western blots with RIC-19 antibodies (Fig. 10 B). However, the cellular localization of RIC-19 was affected by RAB-2. Wild-type and (Q65L)DA mCherry-RAB-2 were able to recruit RIC-19-mYFP to the Golgi in neuronal cell bodies (Fig. 10 C) but not RAB-2(S20N)DN. Particularly RAB-2(Q65L)DA was associated with a very strong localization of RIC-19 at the Golgi and an almost complete absence of the diffusely distributed pool of RIC-19 seen in wild-type RAB-2-expressing motor neurons. Consistently, in both dominant *unc-108* mutants, the localization of RIC-19-mYFP was more confined in neuronal cell bodies as compared with wild type (Fig. 10 D), more strongly in *n501* than in the *n777* mutant. Together, our results suggest that RAB-2 and its effector RIC-19 cooperate during DCV maturation to retain specific cargo in maturing DCVs and prevent its loss to the endosomal-lysosomal system.

## Discussion

### Multiple roles for RAB-2 in membrane trafficking

*C. elegans* and *Drosophila melanogaster* Rab2 are highly enriched in the nervous system (Fig. S1; Zhang et al., 2007; Chun et al., 2008; Mangahas et al., 2008), suggesting a neuronal function. Accordingly, in *C. elegans*, dominant and recessive

expression rescues the axonal NLP-21-YFP levels in *unc-108(n501)* mutants, whereas wild-type levels are not changed. Mean fluorescence was normalized to wild type. (C and D) Overexpression of RAB-5(Q78L)DA leads to the accumulation of NLP-21-YFP in the neuronal cell bodies in the VNC. (B and D) Error bars = SEM (\*\*\*,  $P < 0.005$ ; Student's *t* test). Bars: (A) 10  $\mu$ m; (C) 2  $\mu$ m.

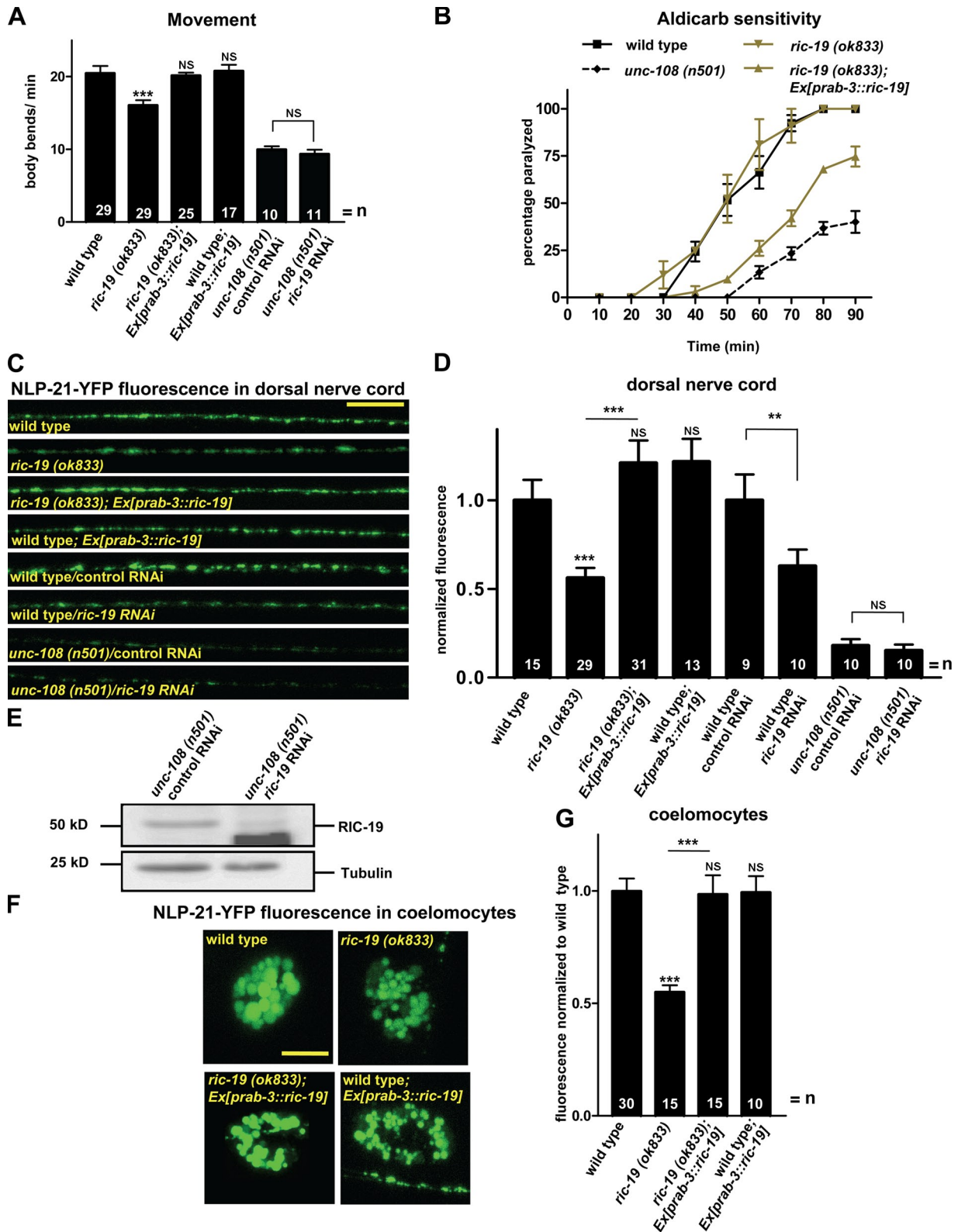
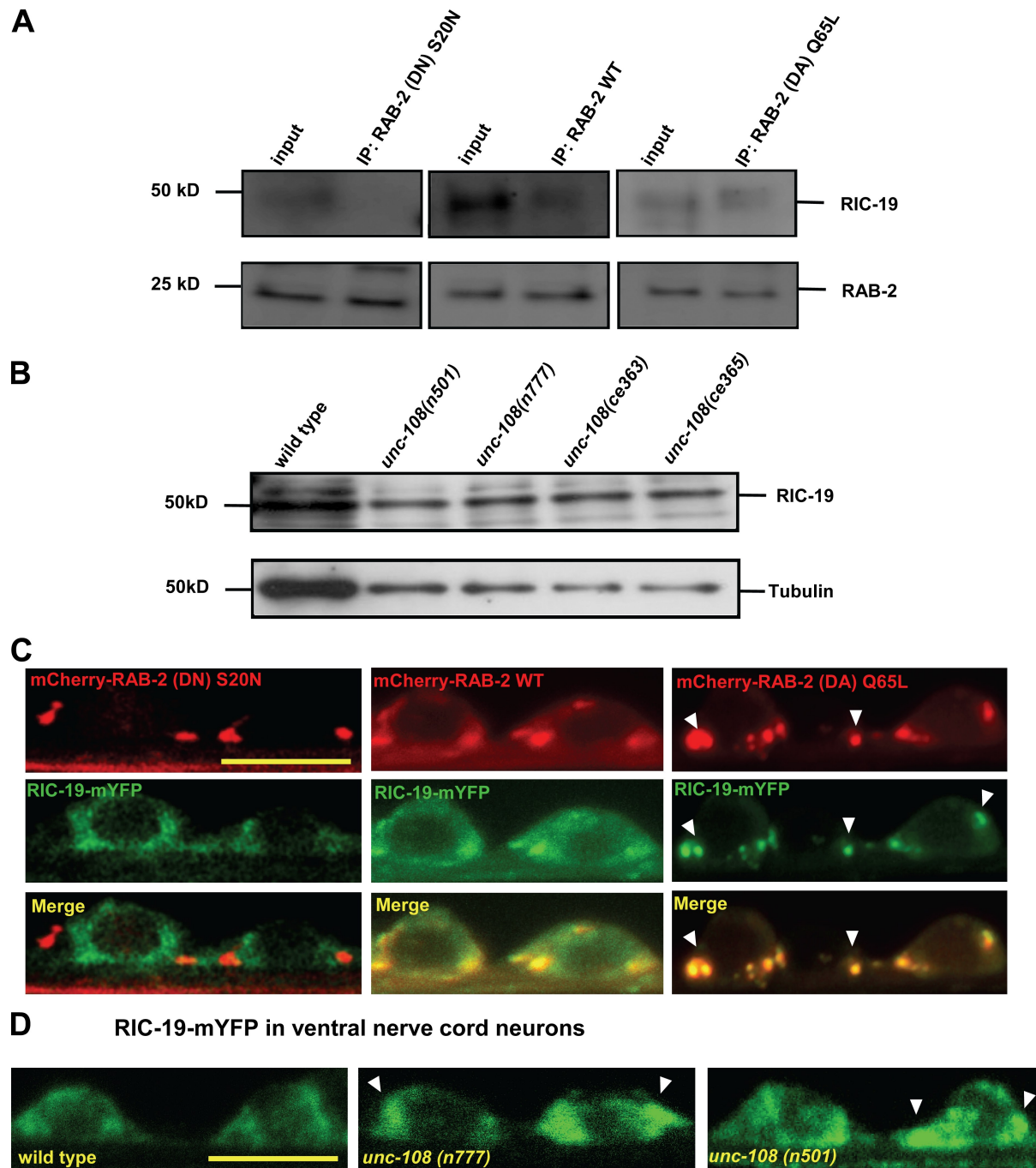


Figure 9. *ric-19* mutants show similar phenotypes to *unc-108* mutants. (A) *ric-19* mutants show movement defects, which can be rescued by neuronal expression of *ric-19*. Knockdown of RIC-19 in *unc-108* has no additional affect on locomotion. (B) *ric-19(ok833)* mutants are resistant to the ACh esterase inhibitor aldicarb, similarly to *unc-108(n501)*. Aldicarb resistance can be rescued by neuronal expression of *ric-19* ( $n = 30$ ). (C and D) *ric-19* deletion or *ric-19* RNAi decreases axonal NLP-21-YFP fluorescence (*nuls183*) similar to *unc-108* mutants. *ric-19* RNAi in *unc-108* mutants shows epistasis. Neuronal expression of RIC-19 rescues DCV defects of *ric-19* mutants. (E) Western blot showing the efficiency of RIC-19 knockdown by RNAi in *unc-108(n501)* mutants. (F and G) *ric-19* mutants secrete less NLP-21-derived YFP (*nuls183*), as measured by coelomocyte fluorescence, which is in agreement with the reduced axonal YFP levels in DCVs. This defect can be rescued by neuronal *ric-19* expression. (A, B, D, and G) Error bars = SEM (\*\*,  $P < 0.01$ ; \*\*\*,  $P < 0.005$ ; Student's *t* test). Bars: (C) 10  $\mu$ m; (F) 5  $\mu$ m.



**Figure 10. The RAB-2 GTP-bound form recruits RIC-19 to the Golgi.** (A) When expressed in HeLa cells, RIC-19 coimmunoprecipitates with wild-type (WT) RAB-2 and its GTP-bound RAB-2(Q65L)DA form but not its inactive GDP-bound RAB-2(S20N)DN form. As a control, the amount of affinity-purified RAB-2 is shown below. IP, immunoprecipitation. (B) Endogenous RIC-19 levels are not altered in *unc-108* mutants, as determined by Western blotting total extracts. (C) RIC-19 localization is mostly cytoplasmic in cells expressing the inactive RAB-2(S20N)DN, but RIC-19 is recruited to Golgi membranes by expression of either wild-type RAB-2 or, to a greater extent, GTP-bound RAB-2(Q65L)DA. Arrowheads show the recruitment of RIC-19 by overexpression of GTP-restricted (DA) RAB-2. (D) As compared with wild-type motor neurons, RIC-19-mYFP shows increased Golgi recruitment in the dominant *unc-108* mutants (marked by arrowheads). Bars, 4  $\mu$ m.

*unc-108/rab-2* mutants display locomotory defects, which are indicative of changes in signaling at the NMJ (Park and Horvitz, 1986; Simmer et al., 2003; Chun et al., 2008; Lu et al., 2008; Mangahas et al., 2008). However, only the recessive loss-of-function alleles are also defective in the removal of apoptotic cells and fluid phase endocytosis in the intestine and coelomocytes as well as glutamate receptor trafficking (Chun et al.,

2008; Lu et al., 2008; Mangahas et al., 2008). This suggests that RAB-2 might be involved in several cellular processes with specific requirements for different levels of RAB-2 activity.

We show that the dominant RAB-2 mutations (*n501*) D122N and (*n777*) S149F, positioned in the conserved G2 and G3 domains that stabilize GTP binding (Fig. 2; Paduch et al., 2001), biochemically behave like the engineered dominant-active

GTP-bound RAB-2(Q65L) protein (Tisdale, 1999). In agreement with this, *rab-2(D122N)* and *rab-2(Q65L)DA* are able to induce locomotion defects when expressed in the neurons of wild-type animals (Chun et al., 2008). Thus, the dominant *rab-2* alleles might still supply enough RAB-2 function for endocytotic trafficking and engulfment events and might therefore be best suited to study the neuronal defects.

#### **RAB-2 affects locomotion through the regulation of DCV signaling**

An extensive HPF EM analysis showed that the synaptic morphology as well as the SV and DCV number and distribution at the NMJ are unaltered in *unc-108* mutants (Fig. 4). We further demonstrated that mutations in RAB-2 specifically affect the maturation but not the release of DCVs. Because *unc-108* mutants have impaired retention of soluble and transmembrane cargo during DCV maturation, a reasonable hypothesis is that neuropeptide function is impaired in *unc-108* mutants, and this may cause the locomotory defect. However, this seems unlikely for several reasons. First, the DCV maturation defect in *unc-108* mutants does not affect the aggregated neuropeptide core of the vesicle (Fig. 4A). Second, the levels of native, processed FMRFamide neuropeptides in the axons of *unc-108* mutants are normal based on antibody staining (Edwards et al., 2009). This is in agreement with a MALDI-TOF MS analysis that showed that neuropeptide processing is not affected in *unc-108* mutants (Table S1). This suggests that functional and processing-competent DCVs are generated. Third, knocking out peptide processing by inactivation of the proprotein convertase EGL-3 in *unc-108* mutants causes a strong synthetic enhancement of the locomotory defect indistinguishable from *unc-31/CAPS* null mutants, which lack DCV release (Fig. 3A). This strongly suggests that most, if not all, neuropeptide function remains intact in *unc-108* null mutants. Therefore, it seems likely that neuropeptides, once aggregated within DCVs, are retained and protected from loss in *unc-108* mutants.

Therefore, the DCV maturation defect in *unc-108* mutants may affect a DCV function unrelated to neuropeptides. One possibility is that RAB-2 affects the sorting of G protein-coupled receptors (GPCRs) and/or their accessory proteins needed for GPCR function and specificity into DCVs (Bermak and Zhou, 2001). Interestingly, expression of dominant Rab2(Q65L) in cell culture and siRNA-mediated down-regulation of Rab2 have been shown to both inhibit cell surface expression and signaling of  $\alpha$ , $\beta$ -adrenergic and angiotensin II type 1 GPCRs (Dong and Wu, 2007). Indeed, the DCV maturation defect in *unc-108* mutants is not restricted to soluble proteins, as the DCV-specific transmembrane protein IDA-1/IA-2 is also affected (Edwards et al., 2009). Another candidate for the missing factor would include soluble neurotrophins or growth factors secreted via the regulated secretory pathway.

Thus, in addition to neuropeptides yet unidentified, GPCRs or growth factors could be cotransported and released from DCVs. Because of the DCV maturation defects in *unc-108* mutants, one or more of these factors may be lost or excluded from *unc-108* DCVs. Thus, we propose that the lack of DCV cargo caused by mistrafficking during DCV maturation results in signaling defects at the NMJ, leading to reduced locomotion.

#### **Molecular function of RAB-2 during DCV maturation**

Rab2 has been shown to regulate vesicular transport and sorting at the Golgi apparatus (Chavrier et al., 1990; Tisdale and Balch, 1996; Tisdale and Jackson, 1998; Tisdale, 1999). Consistently, we were not able to detect RAB-2 at synapses but found it abundantly localized at neuronal Golgi complexes and on vesicular structures surrounding the Golgi and in axons (Fig. 6). Thus, RAB-2 may affect trafficking events that originate at the Golgi or the closely associated endosomal system. DCVs are generated at the late Golgi, most likely within the TGN (Tooze et al., 2001; Kim et al., 2006; Morvan and Tooze, 2008). Here, neuropeptide precursors, processing enzymes, and accessory proteins needed for DCV exocytosis have to be sorted into transport containers that subsequently bud off the Golgi. Our findings that, in *unc-108* mutants, the number of synaptic DCVs as well as the processing of neuropeptides are not affected make it unlikely that RAB-2 is required for the initial generation of iDCV. The fact that, in some recessive alleles, the DCV diameter is more variable and slightly enlarged suggests that RAB-2 might rather affect the fidelity of DCV maturation. In all *unc-108* alleles, we observed DCV cargo NLP-21-YFP to colocalize more strongly with late endosomal and lysosomal markers as compared with wild-type neurons, suggesting that DCV cargo is inappropriately lost from maturing DCVs. Accordingly, the axonal NLP-21-YFP fluorescence intensity could be rescued by blocking early endosomal function through expression of the GTP-bound RAB-5(Q78L) mutant (Fig. 8). This strongly suggests that Rab2 is required to retain specific cargo during DCV maturation.

In addition to proneuropeptides and associated processing enzymes, constitutive secretory cargo, lysosomal enzymes, and other membrane proteins are also copackaged into DCV precursors, forming iDCV budding off the Golgi. To become fully functional, this inappropriate cargo has to be removed from iDCVs by clathrin-mediated remodeling to allow maturation into mDCVs. This proofreading mechanism is important to ensure the generation of mDCVs that contain biologically active neuropeptides and undergo productive membrane fusion (Tooze et al., 2001; Morvan and Tooze, 2008). In particular, after exit from the Golgi apparatus, iDCVs have been reported to undergo syn-6-dependent homotypic fusions to form a functionally distinct compartment from the Golgi (Wendler et al., 2001; Morvan and Tooze, 2008). Later on, syn-6 must be removed from iDCVs because it is no longer detectable on mDCVs. The cargo that is removed from the iDCV compartment by clathrin-coated vesicles is sorted to endosomes (Morvan and Tooze, 2008). We propose that in *unc-108* mutants, this sorting step is affected such that cargo that would normally stay in maturing DCVs, such as soluble cargo-like growth factors or yet unidentified GPCRs, are lost to the endosomal system.

Acidification has also been shown to be important for retention of cargo and processed neuropeptides in maturing iDCVs. Neutralization of acidic compartments causes missorting of mDCV cargo and subsequent secretion from the cell (Moore et al., 1983; Wu et al., 2001). Interestingly, a recessive *unc-108* mutation has been demonstrated to be defective in the acidification of the phagosomal lumen, resulting in engulfment

defects (Mangahas et al., 2008). However, because proprotein convertases are only active under acidic pH conditions (Morvan and Tooze, 2008), severe defects in the acidification of iDCV would also lead to neuropeptide processing defects, which are not observed in *unc-108* mutations (Table S1; Edwards et al., 2009). Therefore, we favor a model in which RAB-2 stabilizes membrane domains required for the retention of cargo in maturing DCVs.

Interestingly, Rab2, has recently been shown to bind to multiple Golgi-localized coiled-coil proteins (Golgins) and Golgi matrix proteins in a GTP-dependent manner (Short et al., 2001; Burguete et al., 2008; Sinka et al., 2008). Golgins mark the identity of specific Golgi regions, whereas Golgi matrix proteins are required to maintain the structural integrity of the Golgi (Panic et al., 2003). The interactions of activated Rab2 with multiple Golgins might confer retention of Rab2-labeled membrane domains in close proximity to the Golgi stack and prevent their diffusion to the cell periphery or endosomes. This local enrichment might also promote homotypic membrane fusion and rearrangement events necessary for efficient maturation (Tooze et al., 2001). Thus, Rab2 could also help to orchestrate a dynamic network of functional interactions required for efficient maturation of DCVs. Because Rab2 is the most highly conserved Rab GTPase, its function for DCV maturation is likely to be conserved throughout evolution.

### RAB-2 cooperates with its effector RIC-19 during DCV maturation

Once activated, Rab GTPases recruit effector molecules to target membranes. Recent work has shown that the diabetes autoantigen ICA69 is a direct Rab2 effector in human insulin-producing  $\beta$  cells. Rab2 recruits ICA69 to Golgi membranes in a GTP-dependent manner (Buffa et al., 2008). The *C. elegans* ICA69 orthologue RIC-19 is specifically expressed in neurons, and *ric-19* mutants are aldicarb resistant (Pilon et al., 2000). In this study, we show that *ric-19* mutants display the same specific DCV maturation defect observed in *unc-108* mutants.

Several lines of evidence suggest that RIC-19 and ICA69 function in a similar process during DCV maturation in cooperation with Rab2. Like ICA69, RIC-19 localizes to the Golgi but not to vesicles (mDCVs or SVs) at the synapse (Spitzenberger et al., 2003). In addition, RIC-19/ICA69 is recruited to the Golgi by activated Rab2 through direct interaction (Spitzenberger et al., 2003). The involvement of ICA69 in DCV maturation is also supported by the fact that ICA69 partially colocalizes with immature secretory granules but dissociates from secretory granule membranes during further maturation (Spitzenberger et al., 2003).

Mechanistically, ICA69/RIC-19 might create or stabilize membrane domains on iDCVs during maturation through its BAR (Bim/amphiphysin/Rvs) domain, which is known to recognize curved membranes found on vesicles and tubular carriers (Habermann, 2004; Zimmerberg and McLaughlin, 2004; Gallop and McMahon, 2005). Several BAR domain-containing homo- and heterodimeric proteins have also been shown to interact with Rab GTPases (Habermann, 2004). The membrane domains generated by ICA69/RIC-19 together with RAB-2 might be necessary to retain specific cargo in iDCVs and prevent their missorting to the endosomal pathway. Although our

data strongly suggest that RIC-19 and RAB-2 act together, we find different requirements for RAB-2 and RIC-19 during DCV maturation. Whereas in *unc-108* mutants the size of DCVs is slightly increased and more variable, it is similar to wild type in *ric-19* mutants. This suggests that Rab2 might have additional functions during DCV maturation. Alternatively, RIC-19 might still be able to associate with iDCV membranes in the absence of RAB-2 via its BAR domain in a curvature-dependent mechanism or through electrostatic interactions with the lipid bilayer. The interaction with RAB-2 might then be specifically required to stabilize these membrane domains to make them productive for sorting and the retention of cargo.

## Materials and methods

### Strains

If not otherwise stated, strains were grown at 20°C as described previously (Brenner, 1974). Strains used in this study were the wild-type Bristol N2 strain, *unc-108(n501)*, *unc-108(n777)*, *ric-19(ok833)*, *rab-3[js49]*, *rrf-3(pk1426)*, *egl-3(gk238)*, *unc-31(e928)*, *lev-10(ok1154)*, *arls37 [pmyo-3::gfp]*, *wyls22 [unc-86::gfp-rab-3]*, *bls34 [prme-8::rme-8-gfp]*, *ccls40 [unc-122::gfp-cup-5]*, *oxls12 [punc-47::gfp]*, and *ccls4251; him-8(e1489)*. *unc-108(ce363)* and *unc-108(ce365)* were provided by K. Miller (Oklahoma Medical Research Foundation, Oklahoma City, OK). *KG1900 unc-108(nu415)*, *nuls152 [punc-129::gfp-snb-1]*, and *nuls183 [punc-129::nlp-21-mvenus]* were provided by J. Kaplan (Massachusetts General Hospital, Boston, MA).

### Behavioral assays

**Movement assay.** To assay locomotion, animals were transferred to Nematode growth medium (NGM) culture plates without food. After an initial adjustment period of 60 min, body bends (corresponding to a whole 360° sine wave) were counted over a 3-min time interval.

**Drug assays.** For the levamisole assay, worms were grown on NGM plates containing levamisole (Sigma-Aldrich) ranging in concentration from 0 to 1 mM in the presence of food (Gally et al., 2004). After 1 h, the number of paralyzed worms was counted. Aldicarb assay was performed as described previously (Mahoney et al., 2006). Worms were grown on plates containing 2 mM aldicarb (Sigma-Aldrich), and the number of paralyzed worms was monitored over a 90-min period in 10-min intervals.

### Expression constructs and markers

The *rab-2* gene was amplified from a cDNA library (ProQuest; Invitrogen), and the Q65L (dominant active) and S20N (dominant inactive) mutations were introduced by site-directed mutagenesis and verified by sequencing. For colocalization experiments, RAB-2 was N-terminally fused to mCherry and expressed under the control of a 1.2-kb *rab-3* promoter fragment. The *ric-19* gene was amplified from the same cDNA library and C-terminally fused to YFP under the *rab-3* promoter. Intracellular markers *prab-3::gfp-cytochrome b5*, *prab-3::manosidase II-gfp*, *prab-3::2xfyve domain-gfp*, and *prab-3::rfp-ecop* were cloned by replacing the *myo-3* promoter from the original vector (Eimer et al., 2007). *rab-3*, *rab-5*, *rab-7*, and *syn-6* cDNAs were amplified by PCR and N-terminally fused to mCherry to generate *prab-3::mCherry-rab-3*, *prab-3::mCherry-rab-5*, *prab-3::mCherry-rab-7*, and *prab-3::mCherry-syn-6*. The coding region of the lysosomal marker *lmp-1* was amplified from genomic DNA and C-terminally fused to mCherry, generating *prab-3::lmp-1-mCherry*. *rab-2(S20N)DN*, *rab-2(Q65L)DA*, and *rab-5(Q78L)DA* were generated by site-directed mutagenesis and N-terminally fused to mCherry to generate *prab-3::mCherry-rab-2(S20N)DN*, *prab-3::mCherry-rab-2(Q65L)DA*, and *prab-3::mCherry-rab-5(Q78L)DA*.

For RNAi experiments, the entire *ric-19* cDNA was cloned into the L4440 multiple cloning site. For *rab-2* expression analysis, a 3.2-kb *rab-2* promoter fragment upstream of the start ATG was amplified from genomic DNA and subcloned as a PstI and KpnI fragment into *pPD115.62 (myo-3::gfp)*, replacing the *myo-3* promoter. For HeLa cell expression, *rab-2* alleles were generated via site-directed mutagenesis and cloned into the multiple cloning site of the *pIRES2-eGFP* vector (Clontech Laboratories, Inc.), whereas *ric-19* was cloned into the *pcDNA4* vector (Invitrogen). All constructs were verified by sequencing.

### Crosses and transgenic strains

Crosses were performed using classical genetic approaches, and the progeny was genotyped by PCR. Table S2 lists all of the strains used and generated in this study. Transgenic strains were generated by microinjection as previously described (Mello et al., 1991). The injection mixes were adjusted to a total DNA concentration of 100 ng/ $\mu$ l by the addition of *pBlue-Script SKII* (Agilent Technologies). Table S3 lists all of the transgenic strains generated for this study, including the plasmid and coinjection marker concentration.

### Fluorescence imaging and quantitative analysis

Live animals were placed on 2% agarose pads and immobilized with 50 mM Na-azide in M9 buffer. All images were obtained on an inverted confocal microscope (SP2; Leica) using a 63 $\times$  NA 1.32 oil immersion objective at 20°C. Image stacks were captured, and maximum intensity projections were obtained using Confocal software (Leica).

For localization experiments, images of neuronal cell bodies in the VNC were taken. For the DNC experiments, images were obtained as described previously (Sieburth et al., 2007). The posterior part of the DNC was imaged in young adult animals when oriented toward the objective, using the same settings for all of the images obtained. For the coelomocyte imaging, the posterior coelomocyte was imaged in young adults when oriented laterally. Maximum stack projections were thresholded and analyzed using ImageJ software (National Institutes of Health) as described previously (Sieburth et al., 2007). For the vesicular structure diameter quantification, stacks through entire cells were obtained using the same magnification for all cells, and the diameter was determined for each vesicle observed using ImageJ software. The data were analyzed in ImageJ software and normalized to wild type.

### Protein expression, purification, and Western blotting

The *rab-2* cDNA was cloned into *pGST parallel 1* vector (Sheffield et al., 1999). The protein was produced in *Escherichia coli* BL21 star (DE3) strain (Invitrogen) by inducing expression with 1 mM IPTG. GST fusion proteins were purified by selective binding to glutathione Sepharose (GE Healthcare) according to the manufacturer's protocol. Purified proteins were dialyzed against PBS buffer. For RAB-2 and RIC-19 protein quantification, mixed staged worm extracts were prepared as reported previously (Eimer et al., 2007). Mixed staged worms were rinsed in a large (9 cm) plate using PBS buffer, washed four times with PBS, pelleted by centrifugation, and shock frozen in liquid nitrogen. The worm pellet was ground under liquid nitrogen to fine powder in a ceramic mortar. Before 1 $\times$  SDS buffer was added, a 10- $\mu$ l sample was used to estimate the total protein concentration using a Bradford assay. 15  $\mu$ g of total protein extract per strain was loaded and separated on 15% SDS-polyacrylamide gel, blotted onto nitrocellulose membrane, and probed against RAB-2 and RIC-19 (provided by M. Pilon, University of Gothenburg, Gothenburg, Sweden; Pilon et al., 2000) primary antibody using 1:2,000 and 1:5,000 dilutions, respectively, and peroxidase-coupled secondary antibodies (The Jackson Laboratory). The signal was revealed with Super Signal West Dura substrate (Thermo Fisher Scientific) and quantified using ImageJ software. The data were normalized to tubulin.

### Antibody production

10 mice were immunized with 50  $\mu$ g of purified fusion protein in PBS using complete Freund's adjuvant (Sigma-Aldrich). Booster injections were given thereafter every 4th wk with the same amount of antigen in incomplete Freund's adjuvant (Sigma-Aldrich). 30 d after the last injection, the whole blood was collected. To obtain polyclonal mouse antibodies against RAB-2, the sera were combined and affinity purified against RAB-2 fusion protein as reported previously (Eimer et al., 2007). Monoclonal antibodies against RAB-2 were generated subsequently according to standard protocols.

### Cell culture

HeLa cells were grown in DME supplemented with 10% FBS, 2 mM glutamine, 100 U/ml penicillin, and 10  $\mu$ g/ml streptomycin in a 5% CO<sub>2</sub> incubator at 37°C. Cells were transfected in 35-mm tissue culture dishes as described previously (Sambrook and Russell, 2001). After 16 h, cells were washed in PBS, collected in PBS buffer containing 10 mM EDTA, and extracted in lysis buffer (50 mM Hepes, pH 7.4, 1% Triton X-100, 100 mM NaCl, 5 mM MgCl<sub>2</sub>, 1 mM PMSF, and 10 mM Na-phosphate) for 20 min at 4°C. The protein extracts were loaded and analyzed on 15% SDS-polyacrylamide gel. Immunoprecipitation was performed as described previously (Buffa et al., 2008). HA-tagged RAB-2 proteins were expressed in HeLa cells and upon cell lysis in lysis buffer (50 mM Tris-HCl, pH 8.0, 150 mM NaCl, 1% Triton X-100, and 1% protease inhibitor cocktail) and precipitated overnight with red anti-HA affinity gel (Sigma-Aldrich) at 4°C.

Beads were washed with washing buffer (50 mM Tris-HCl, pH 7.4, 300 mM NaCl, 0.1% Triton X-100, 5 mM EDTA, and 0.02% Na-azide), and protein was eluted from the beads with SDS sample buffer and analyzed on SDS-polyacrylamide gels.

### GTPase and GTP affinity assays

The GTPase assay was performed as previously described (Spinosa et al., 2008). Purified proteins were dialyzed in buffer A (20 mM Tris-HCl, pH 7.8, 100 mM NaCl, 5 mM MgCl<sub>2</sub>, 1 mM Na-phosphate, and 10 mM 2-mercaptoethanol) and incubated with glutathione agarose (Thermo Fisher Scientific) for 2 h at 4°C. Bound nucleotide was eluted washing once with buffer C (20 mM Tris-HCl, pH 7.8, 100 mM NaCl, 5 mM MgCl<sub>2</sub>, 1 mM Na-phosphate, 2 mM EDTA, and 10 mM 2-mercaptoethanol) and then twice in ice-cold buffer A. 1 pmol of immobilized GST-tagged proteins was then mixed with 1 pmol  $\alpha$ -[<sup>32</sup>P]GTP in 20  $\mu$ l of buffer A and incubated at 4°C for 10 min. 50  $\mu$ l of buffer A was added to each sample, and aliquots were taken at various time points. After incubation, proteins were washed three times in buffer A, and 8  $\mu$ l of buffer B was added (0.2% SDS, 2 mM EDTA, 10 mM GDP, and 10 mM GTP, pH 7.5). The samples were heated at 70°C, and 2- $\mu$ l aliquots were spotted on polyethyleneimine cellulose membrane for thin-layer chromatography in 0.6 mM of Na-phosphate buffer, pH 3.5, and the radioactivity spots were visualized and analyzed using ImageJ software. GTP affinity assay was performed as previously described (Shapiro et al., 1993). 100 nM of GST-RAB-2 proteins was incubated with 2  $\mu$ M  $\gamma$ -[<sup>35</sup>S]GTP for 6 h at room temperature. Subsequently, 100-fold excess of unlabeled GTP was added, and aliquots were collected at various time points. The bound radioactivity was analyzed in samples taken at the indicated time points.

### EM

HPF and freeze substitution were performed as previously described (Rostaing et al., 2004). For morphological investigations, 50-nm sections were analyzed, and for immuno-EM, 85-nm sections were labeled (Weimer et al., 2006) with 1:50 anti-RAB-2 mouse serum and 1:100 monoclonal anti-GFP antibody (Roche). Micrographs were taken with a 1,024  $\times$  1,024-pixel charge-coupled device detector (Proscan CCD HSS 512/1024; Proscan Electronic Systems) in an electron micrograph (EM 902A; Carl Zeiss, Inc.) operated in the bright field mode. The SV and DCV diameter and distribution at the synapse of motor neurons were analyzed by a semiautomated analysis software, which is now available on our homepage.

### Quantitative EM measurement and immuno-EM

The SV and DCV diameter and distribution at the synapse of motor neurons were analyzed by a semiautomated analysis software XtraCount, which is available on our homepage (<http://www.eni.gwdg.de/index.php?id=316>). One profile per synapse was analyzed. SVs were allocated to bins of 50 nm extending from the presynaptic density into the cytoplasm and displayed as a percentage of vesicles per bin. Vesicle diameters were analyzed using the same program, but the middle of the membrane bilayer was used as vesicle limits.

### Electrophysiology

The worm dissection was performed as previously described (Richmond et al., 1999). In brief, animals were immobilized with cyanoacrylate glue, and a lateral cuticle incision was made, exposing the ventral medial body wall muscles. Muscle recordings were made in the whole cell voltage-clamp configuration (holding potential of -60 mV) using an EPC-10 patch-clamp amplifier (HEKA) and digitized at 1 kHz. The extracellular  $\sim$ 340-mosM solution, pH 7.3, consisted of 150 mM NaCl, 5 mM KCl, 5 mM CaCl<sub>2</sub>, 4 mM MgCl<sub>2</sub>, 10 mM glucose, 5 mM sucrose, and 15 mM Hepes. The patch pipette was filled with an  $\sim$ 315-mosM solution, pH 7.2, of 120 mM KCl, 20 mM KOH, 4 mM MgCl<sub>2</sub>, 5 mM N-tris(Hydroxymethyl) methyl-2-aminoethanesulfonic acid, 0.25 mM CaCl<sub>2</sub>, 4 mM Na<sup>2</sup>ATP, 36 mM sucrose, and 5 mM EGTA. Postsynaptic responses were evoked using a 2-ms depolarizing pulse delivered from a stimulating electrode placed against the VNC  $\sim$ 100  $\mu$ m anterior to the clamped muscle cell. Data were acquired using Pulse software (HEKA) run on a Dell computer. Subsequent analysis and graphing was performed using Pulsefit (HEKA) and Igor Pro (WaveMetrics).

### RNAi

RNAi by feeding was performed as previously described (Kamath et al., 2001). L4440 vector caring the *ric-19* gene or the empty L4440 vector was transformed into *E. coli* HT115 (DE3) strain. The overnight culture, grown in Luria broth media with 100  $\mu$ g/ml ampicillin, was used for seeding NGM plates containing 50  $\mu$ g/ml ampicillin and 1 mM IPTG. 10 L4 larvae of strains with *rrf-3* mutant background were transferred onto the

plates, left to lay eggs for 12 h, and then transferred to a new plate. The progeny was analyzed.

### Peptidomics

Endogenous peptides were extracted using a slightly modified protocol as previously described (Husson et al., 2005). In brief, mixed staged animals were extracted in ice-cold extraction solvent (methanol/water/acetic acid, 90:9:1) and homogenized by sonification. The methanol was evaporated, and the aqueous solution was reextracted with ethyl acetate and *n*-hexane to remove the lipids. Finally, the peptide extract was desalted, lyophilized, and reconstituted in 500  $\mu$ l of water containing 4% CH<sub>3</sub>CN and 0.1% trifluoroacetic acid (TFA) and filtered (22  $\mu$ m; Ultrafree-MC; Millipore). Peptides were separated on a column (2.1  $\times$  150 mm; 3.5  $\mu$ m; Symmetry C18; Waters) using a linear gradient from 4% CH<sub>3</sub>CN in 0.1% aqueous TFA to 52% CH<sub>3</sub>CN in 0.1% aqueous TFA in 60 min at a flow rate of 300  $\mu$ l/min to generate 60 fractions. The peptide content of each fraction was monitored by MALDI-TOF MS on an Ultraflex II instrument (Bruker Daltonics, GmbH).

### Online supplemental material

Fig. S1 shows the expression pattern analysis of *unc-108/rab-2*. Fig. S2 shows that *unc-108/rab-2* mutants exhibit a normal neuronal development and synaptic pattern. Fig. S3 shows that the morphology of the Golgi apparatus is not affected in *unc-108/rab-2* mutants. Fig. S4 shows that *ric-19* mutant neuronal cell bodies accumulate abnormally large vesicular structures positive for the NLP-21-YFP-derived fusion protein. Fig. S5 shows the analysis of coelomocyte morphology and functionality of fluid phase uptake in *unc-108/rab-2* mutants. Table S1 shows the high performance liquid chromatography–MALDI-TOF MS analysis of neuropeptides in wild type and *unc-108* mutants. Tables S2 and S3 list the strains and transgenic arrays, respectively, used in this study. Online supplemental material is available at <http://www.jcb.org/cgi/content/full/jcb.200902096/DC1>.

We thank Francis Barr for the hRab2 cDNA, Shweta Aggarwal, Reinhard Jahn, and Gottfried Mieskes for support, Marc Pilon for RIC-19 antibodies, Ken Miller and Josh Kaplan for strains, and Ken Miller for sharing unpublished results and discussions. We specially thank Virginie Lecaudey, Nikhil Sasidharan, and Reinhard Jahn for their comments on the manuscript. Some strains were provided by the *Caenorhabditis* Genetics Center, which is supported by the National Institutes of Health National Center for Research Resources.

We gratefully acknowledge funding by the European Union (EU) Sixth Framework Programme coordination action program European Network of Neuroscience Institutes, Neuroscience Early Stage Research Training fellowships of the EU to L. Luo and M. Sumakovic, and a postdoctoral fellowship from the Research Foundation Flanders (FWO) to S.J. Husson. L. Schoofs is supported by the FWO, and S. Eimer is supported by the German Research Foundation Research Center for Molecular Physiology of the Brain.

Submitted: 18 February 2009

Accepted: 27 August 2009

## References

- Bermak, J.C., and Q.Y. Zhou. 2001. Accessory proteins in the biogenesis of G protein-coupled receptors. *Mol. Interv.* 1:282–287.
- Brenner, S. 1974. The genetics of *Caenorhabditis elegans*. *Genetics*. 77:71–94.
- Buffa, L., E. Fuchs, M. Pietropaolo, F. Barr, and M. Solimena. 2008. ICA69 is a novel Rab2 effector regulating ER-Golgi trafficking in insulinoma cells. *Eur. J. Cell Biol.* 87:197–209. doi:10.1016/j.ejcb.2007.11.003
- Burguete, A.S., T.D. Fenn, A.T. Brunger, and S.R. Pfeffer. 2008. Rab and Arl GTPase family members cooperate in the localization of the golgin GCC185. *Cell*. 132:286–298. doi:10.1016/j.cell.2007.11.048
- Chavrier, P., R.G. Parton, H.P. Hauri, K. Simons, and M. Zerial. 1990. Localization of low molecular weight GTP binding proteins to exocytic and endocytic compartments. *Cell*. 62:317–329. doi:10.1016/0092-8674(90)90369-P
- Chun, D.K., J.M. McEwen, M. Burbea, and J.M. Kaplan. 2008. UNC-108/Rab2 regulates postendocytic trafficking in *Caenorhabditis elegans*. *Mol. Biol. Cell*. 19:2682–2695. doi:10.1091/mbc.E07-11-1120
- Dong, C., and G. Wu. 2007. Regulation of anterograde transport of adrenergic and angiotensin II receptors by Rab2 and Rab6 GTPases. *Cell. Signal.* 19:2388–2399. doi:10.1016/j.cellsig.2007.07.017
- Edwards, S.L., N.K. Charlie, J.E. Richmond, J. Hegermann, S. Eimer, and K.G. Miller. 2009. Impaired dense core vesicle maturation in *Caenorhabditis elegans* mutants lacking Rab2. *J. Cell Biol.* 186:881–895.
- Eimer, S., A. Gottschalk, M. Hengartner, H.R. Horvitz, J. Richmond, W.R. Schafer, and J.L. Bessereau. 2007. Regulation of nicotinic receptor trafficking by the transmembrane Golgi protein UNC-50. *EMBO J.* 26:4313–4323. doi:10.1038/sj.emboj.7601858
- Fukuda, M. 2008. Regulation of secretory vesicle traffic by Rab small GTPases. *Cell. Mol. Life Sci.* 65:2801–2813. doi:10.1007/s00018-008-8351-4
- Gallop, J.L., and H.T. McMahon. 2005. BAR domains and membrane curvature: bringing your curves to the BAR. *Biochem. Soc. Symp.* 72:223–231.
- Gally, C., S. Eimer, J.E. Richmond, and J.L. Bessereau. 2004. A transmembrane protein required for acetylcholine receptor clustering in *Caenorhabditis elegans*. *Nature*. 431:578–582. doi:10.1038/nature02893
- Gracheva, E.O., A.O. Burdina, D. Touroutine, M. Berthelot-Grosjean, H. Parekh, and J.E. Richmond. 2007. Tomosyn negatively regulates CAPS-dependent peptide release at *Caenorhabditis elegans* synapses. *J. Neurosci.* 27:10176–10184. doi:10.1523/JNEUROSCI.2339-07.2007
- Gracheva, E.O., G. Hadwiger, M.L. Nonet, and J.E. Richmond. 2008. Direct interactions between *C. elegans* RAB-3 and Rim provide a mechanism to target vesicles to the presynaptic density. *Neurosci. Lett.* 444:137–142. doi:10.1016/j.neulet.2008.08.026
- Habermann, B. 2004. The BAR-domain family of proteins: a case of bending and binding? *EMBO Rep.* 5:250–255. doi:10.1038/sj.embor.7400105
- Husson, S.J., E. Clynen, G. Baggerman, A. De Loof, and L. Schoofs. 2005. Discovering neuropeptides in *Caenorhabditis elegans* by two dimensional liquid chromatography and mass spectrometry. *Biochem. Biophys. Res. Commun.* 335:76–86. doi:10.1016/j.bbrc.2005.07.044
- Husson, S.J., E. Clynen, G. Baggerman, T. Janssen, and L. Schoofs. 2006. Defective processing of neuropeptide precursors in *Caenorhabditis elegans* lacking proprotein convertase 2 (KPC-2/EGL-3): mutant analysis by mass spectrometry. *J. Neurochem.* 98:1999–2012. doi:10.1111/j.1471-4159.2006.04014.x
- Husson, S.J., T. Janssen, G. Baggerman, B. Bogert, A.H. Kahn-Kirby, K. Ashrafi, and L. Schoofs. 2007a. Impaired processing of FLP and NLP peptides in carboxypeptidase E (EGL-21)-deficient *Caenorhabditis elegans* as analyzed by mass spectrometry. *J. Neurochem.* 102:246–260. doi:10.1111/j.1471-4159.2007.04474.x
- Husson, S.J., I. Mertens, T. Janssen, M. Lindemans, and L. Schoofs. 2007b. Neuropeptidergic signaling in the nematode *Caenorhabditis elegans*. *Prog. Neurobiol.* 82:33–55. doi:10.1016/j.pneurobio.2007.01.006
- Kamath, R.S., M. Martinez-Campos, P. Zipperlen, A.G. Fraser, and J. Ahringer. 2001. Effectiveness of specific RNA-mediated interference through ingested double-stranded RNA in *Caenorhabditis elegans*. *Genome Biol.* 2:research0002.1–0002.10.
- Kass, J., T.C. Jacob, P. Kim, and J.M. Kaplan. 2001. The EGL-3 proprotein convertase regulates mechanosensory responses of *Caenorhabditis elegans*. *J. Neurosci.* 21:9265–9272.
- Kim, T., M.C. Gondré-Lewis, I. Arnaoutova, and Y.P. Loh. 2006. Dense-core secretory granule biogenesis. *Physiology (Bethesda)*. 21:124–133.
- Li, C., L.S. Nelson, K. Kim, A. Nathoo, and A.C. Hart. 1999. Neuropeptide gene families in the nematode *Caenorhabditis elegans*. *Ann. N. Y. Acad. Sci.* 897:239–252. doi:10.1111/j.1749-6632.1999.tb07895.x
- Lu, Q., Y. Zhang, T. Hu, P. Guo, W. Li, and X. Wang. 2008. *C. elegans* Rab GTPase 2 is required for the degradation of apoptotic cells. *Development*. 135:1069–1080. doi:10.1242/dev.016063
- Mahoney, T.R., Q. Liu, T. Itoh, S. Luo, G. Hadwiger, R. Vincent, Z.W. Wang, M. Fukuda, and M.L. Nonet. 2006. Regulation of synaptic transmission by RAB-3 and RAB-27 in *Caenorhabditis elegans*. *Mol. Biol. Cell*. 17:2617–2625. doi:10.1091/mbc.E05-12-1170
- Mangahas, P.M., X. Yu, K.G. Miller, and Z. Zhou. 2008. The small GTPase Rab2 functions in the removal of apoptotic cells in *Caenorhabditis elegans*. *J. Cell Biol.* 180:357–373. doi:10.1083/jcb.200708130
- Mello, C.C., J.M. Kramer, D. Stinchcomb, and V. Ambros. 1991. Efficient gene transfer in *C. elegans*: extrachromosomal maintenance and integration of transforming sequences. *EMBO J.* 10:3959–3970.
- Miller, K.G., A. Alfonso, M. Nguyen, J.A. Crowell, C.D. Johnson, and J.B. Rand. 1996. A genetic selection for *Caenorhabditis elegans* synaptic transmission mutants. *Proc. Natl. Acad. Sci. USA*. 93:12593–12598. doi:10.1073/pnas.93.22.12593
- Moore, H.P., B. Gumbiner, and R.B. Kelly. 1983. Chloroquine diverts ACTH from a regulated to a constitutive secretory pathway in AtT-20 cells. *Nature*. 302:434–436. doi:10.1038/302434a0
- Morvan, J., and S.A. Tooze. 2008. Discovery and progress in our understanding of the regulated secretory pathway in neuroendocrine cells. *Histochem. Cell Biol.* 129:243–252. doi:10.1007/s00418-008-0377-z
- Ng, E.L., and B.L. Tang. 2008. Rab GTPases and their roles in brain neurons and glia. *Brain Res. Rev.* 58:236–246. doi:10.1016/j.brainresrev.2008.04.006
- Paduch, M., F. Jelen, and J. Otlewski. 2001. Structure of small G proteins and their regulators. *Acta Biochim. Pol.* 48:829–850.
- Panic, B., O. Perisic, D.B. Veprintsev, R.L. Williams, and S. Munro. 2003. Structural basis for Arl1-dependent targeting of homodimeric

- GRIP domains to the Golgi apparatus. *Mol. Cell.* 12:863–874. doi:10.1016/S1097-2765(03)00356-3
- Park, E.C., and H.R. Horvitz. 1986. Mutations with dominant effects on the behavior and morphology of the nematode *Caenorhabditis elegans*. *Genetics.* 113:821–852.
- Pilon, M., X.R. Peng, A.M. Spence, R.H. Plasterk, and H.M. Dosch. 2000. The diabetes autoantigen ICA69 and its *Caenorhabditis elegans* homologue, ric-19, are conserved regulators of neuroendocrine secretion. *Mol. Biol. Cell.* 11:3277–3288.
- Richmond, J.E., and E.M. Jorgensen. 1999. One GABA and two acetylcholine receptors function at the *C. elegans* neuromuscular junction. *Nat. Neurosci.* 2:791–797. doi:10.1038/12160
- Richmond, J.E., W.S. Davis, and E.M. Jorgensen. 1999. UNC-13 is required for synaptic vesicle fusion in *C. elegans*. *Nat. Neurosci.* 2:959–964. doi:10.1038/12160
- Rostaing, P., R.M. Weimer, E.M. Jorgensen, A. Triller, and J.L. Bessereau. 2004. Preservation of immunoreactivity and fine structure of adult *C. elegans* tissues using high-pressure freezing. *J. Histochem. Cytochem.* 52:1–12.
- Sambrook, J., and D.W. Russell. 2001. Calcium-phosphate-mediated transfection of cells with high-molecular-weight genomic DNA. In *Molecular Cloning: A Laboratory Manual*. Third edition. Cold Spring Harbor Laboratory Press, Cold Spring Harbor, NY. 16.21–16.24.
- Shapiro, A.D., M.A. Riederer, and S.R. Pfeffer. 1993. Biochemical analysis of rab9, a ras-like GTPase involved in protein transport from late endosomes to the trans Golgi network. *J. Biol. Chem.* 268:6925–6931.
- Sheffield, P., S. Garrard, and Z. Derewenda. 1999. Overcoming expression and purification problems of RhoGDI using a family of “parallel” expression vectors. *Protein Expr. Purif.* 15:34–39. doi:10.1006/prep.1998.1003
- Short, B., C. Preisinger, R. Körner, R. Kopajtich, O. Byron, and F.A. Barr. 2001. A GRASP55-rab2 effector complex linking Golgi structure to membrane traffic. *J. Cell Biol.* 155:877–883. doi:10.1083/jcb.200108079
- Sieburth, D., J.M. Madison, and J.M. Kaplan. 2007. PKC-1 regulates secretion of neuropeptides. *Nat. Neurosci.* 10:49–57. doi:10.1038/nn1810
- Simmer, F., C. Moorman, A.M. van der Linden, E. Kuijk, P.V. van den Berghe, R.S. Kamath, A.G. Fraser, J. Ahringer, and R.H. Plasterk. 2003. Genome-wide RNAi of *C. elegans* using the hypersensitive rrf-3 strain reveals novel gene functions. *PLoS Biol.* 1:E12. doi:10.1371/journal.pbio.0000012
- Sinka, R., A.K. Gillingham, V. Kondylis, and S. Munro. 2008. Golgi coiled-coil proteins contain multiple binding sites for Rab family G proteins. *J. Cell Biol.* 183:607–615. doi:10.1083/jcb.200808018
- Spinosa, M.R., C. Progida, A. De Luca, A.M. Colucci, P. Alifano, and C. Bucci. 2008. Functional characterization of Rab7 mutant proteins associated with Charcot-Marie-Tooth type 2B disease. *J. Neurosci.* 28:1640–1648. doi:10.1523/JNEUROSCI.3677-07.2008
- Spitzenberger, F., S. Pietropaolo, P. Verkade, B. Habermann, S. Lacas-Gervais, H. Mziaut, M. Pietropaolo, and M. Solimena. 2003. Islet cell autoantigen of 69 kDa is an arfaptin-related protein associated with the Golgi complex of insulinoma INS-1 cells. *J. Biol. Chem.* 278:26166–26173. doi:10.1074/jbc.M21322200
- Star, E.N., A.J. Newton, and V.N. Murthy. 2005. Real-time imaging of Rab3a and Rab5a reveals differential roles in presynaptic function. *J. Physiol.* 569:103–117. doi:10.1113/jphysiol.2005.092528
- Takamori, S., M. Holt, K. Stenius, E.A. Lemke, M. Grønborg, D. Riedel, H. Urlaub, S. Schenck, B. Brügger, P. Ringler, et al. 2006. Molecular anatomy of a trafficking organelle. *Cell.* 127:831–846. doi:10.1016/j.cell.2006.10.030
- Tisdale, E.J. 1999. A Rab2 mutant with impaired GTPase activity stimulates vesicle formation from pre-Golgi intermediates. *Mol. Biol. Cell.* 10:1837–1849.
- Tisdale, E.J., and W.E. Balch. 1996. Rab2 is essential for the maturation of pre-Golgi intermediates. *J. Biol. Chem.* 271:29372–29379. doi:10.1074/jbc.271.46.29372
- Tisdale, E.J., and M.R. Jackson. 1998. Rab2 protein enhances coatamer recruitment to pre-Golgi intermediates. *J. Biol. Chem.* 273:17269–17277. doi:10.1074/jbc.273.27.17269
- Tooze, S.A., G.J. Martens, and W.B. Huttner. 2001. Secretory granule biogenesis: rafting to the SNARE. *Trends Cell Biol.* 11:116–122. doi:10.1016/S0962-8924(00)01907-3
- Weimer, R.M., E.O. Gracheva, O. Meyrignac, K.G. Miller, J.E. Richmond, and J.L. Bessereau. 2006. UNC-13 and UNC-10/rim localize synaptic vesicles to specific membrane domains. *J. Neurosci.* 26:8040–8047. doi:10.1523/JNEUROSCI.2350-06.2006
- Wendler, F., L. Page, S. Urbé, and S.A. Tooze. 2001. Homotypic fusion of immature secretory granules during maturation requires syntaxin 6. *Mol. Biol. Cell.* 12:1699–1709.
- Wu, M.M., M. Grabe, S. Adams, R.Y. Tsien, H.P. Moore, and T.E. Machen. 2001. Mechanisms of pH regulation in the regulated secretory pathway. *J. Biol. Chem.* 276:33027–33035. doi:10.1074/jbc.M103917200
- Zerial, M., and H. McBride. 2001. Rab proteins as membrane organizers. *Nat. Rev. Mol. Cell Biol.* 2:107–117. doi:10.1038/35052055
- Zhang, J., K.L. Schulze, P.R. Hiesinger, K. Suyama, S. Wang, M. Fish, M. Acar, R.A. Hoskins, H.J. Bellen, and M.P. Scott. 2007. Thirty-one flavors of *Drosophila* rab proteins. *Genetics.* 176:1307–1322. doi:10.1534/genetics.106.066761
- Zimmerberg, J., and S. McLaughlin. 2004. Membrane curvature: how BAR domains bend bilayers. *Curr. Biol.* 14:R250–R252. doi:10.1016/j.cub.2004.02.060